Using remote sensing to quantify albedo of roofs in seven California cities

Final Report to

CALIFORNIA AIR RESOURCES BOARD

Project # 10-321

Prepared by:

Dr. George Ban-Weiss

Jordan Woods

Dr. Ronnen Levinson

Environmental Energy Technologies Division
Lawrence Berkeley National Laboratory
One Cyclotron Road
Berkeley, CA 94720

March 2014

Disclaimer

The statements and conclusions in this report are those of the contractor and not necessarily those of the California Air Resources Board. The mention of commercial products, their source, or their use in connection with material reported herein is not to be construed as actual or implied endorsement of such products.

We note that results summarized in this report will also be published as two peer-reviewed journal articles:

Ban-Weiss GA, Woods J, Levinson R, (submitted) Using remote sensing to quantify albedo of roofs in seven California cities, Part 1: Methods.

Ban-Weiss GA, Woods J, Millstein D, Levinson R (submitted). Using remote sensing to quantify albedo of roofs in seven California cities, Part 2: Results and application to climate modeling.

Acknowledgements

The authors thank the California Air Resources Board for funding this project under Contract 10-321. We especially thank Ash Lashgari, Eileen McCauley, and Tony VanCuren of the California Air Resources Board.

We also thank Doug Cain of North West Group; Dev Millstein of Lawrence Berkeley Lab for performing WRF simulations; Sharon Chen, Pablo Rosado, Ben Mandel, and Ling Jin of Lawrence Berkeley National Laboratory; and Ana Paula Werle of Universidade de São Paulo. For rooftop access we thank John Skyberg and Christopher Brown of San Jose State University; Leroy Sisneros and Fran Knight of University of California, Los Angeles; Chet Galland of California State University, Northridge; Craig Meyer of Pierce College; Victor Lai and Charles A. Meyer of San Francisco State University; and John Zertuche, Cynthia Kranc, and Jon Wildberger of University of California, Davis. For roof installation data we thank CertainTeed; Joe Mellott, Tom Chapman, Amy Digby, and Sean Gavin of The Garland Company, Inc; Michael Kearney of GAF; Tony Zaffuto of Sylvester Roofing Co. Inc.; and Emmie Limon of SureCoat Systems. For assistance obtaining building outlines we thank Vicky Gallardo at City of San Jose, Mark Greninger at County of Los Angeles, and Craig Tranby at Los Angeles Department of Water & Power.

This project was funded by the California Air Resources Board under Contract 10-321. It was also supported by the Assistant Secretary for Energy Efficiency and Renewable Energy, Office of Building Technology, State, and Community Programs, of the U.S. Department of Energy under Contract No. DE-AC02-05CH11231. The statements and conclusions in this report are those of the authors and not necessarily those of the California Air Resources Board.

Table of Contents

Disclaimer II
Acknowledgements III
List of Figures VI
List of Tables IX
List of Acronyms, Initialisms, and Symbols X
Abstract XII
1. Executive Summary 1
2. Introduction 3
3. Developing the Methods 6
3.1. Methods 6
3.1.1 Data source 6
3.1.2 Correcting for the atmosphere and bidirectional reflectance distribution 7
3.1.3 Extracting roof pixels from the imagery 8
3.1.4 Relating albedo to narrowband reflectances 8
3.1.5 Calibrating remotely sensed albedos using ground truths 9
3.1.6 Mean albedo for each roof 11
3.1.7 Precision of the remotely sensed albedos 11
3.2. Results 12
3.2.1 Obtaining solar reflectance (albedo) from remotely sensed (narrowband) reflectances 12
3.2.2 Calibrating remotely sensed albedos using ground truths 13
3.2.3 Maps of roof albedo 13
3.2.4 Discussion and Conclusions 14
4. City-wide results and application to climate modeling 26
4.1. Overview 26
4.2. Results 26
4.2.1 Roof albedos for Los Angeles, Long Beach, Bakersfield, San Francisco, and San Jose 26
4.2.2 Roof albedos in Sacramento and San Diego 27
4.2.3 Precision of the remotely sensed albedos 28
4.3. Discussion 28

4.3.1 Disaggregating roof albedos by roof area 28
4.3.2 Computing the fraction of large roofs that have high albedo 29
4.4. Application: Predicting regional temperature changes from cool roofs 29
4.4.1 Modeling setup 30
4.4.2 Computing albedos for the ‘base_case’ and ‘cool_roof’ scenarios 30
4.4.3 Comparing ‘base_case’ scenario simulations to observations 32
4.4.4 Simulated changes in surface air temperature from cool roofs 32
4.4.5 Simulated changes in precipitation from cool roofs 33
5. Summary and conclusions 57
5.1. Future Research 58
6. References 59
Appendix A. Estimating the potential for cool roofs to increase urban albedo 65
Appendix B. Brief summary of cool roof requirements in California 66

List of Figures

Figure 3-1. Schematic of our approach for deriving the mean albedo of individual roofs from the aerial imagery. 18

Figure 3-2. Examples of the 1 m resolution remotely sensed imagery for a portion of San Jose, California, showing reflectance in four narrow bands: (a) blue (420 – 492 nm), (b) green (533 – 587 nm), (c) red (604 – 664 nm), and (d) near-IR (833 – 920 nm). 19

Figure 3-3. Example building outlines. Outlines provided by the City of San Jose are shown in (a) and (b). Manually traced outlines in Sacramento are in (c). In (a) and (c) the underlying imagery is an RGB composite of the aerial imagery described in this report. In (b) the underlying imagery (source = United States Geological Survey) is higher spatial resolution to help distinguish fine-scale features; this imagery but not radiometerically calibrated. 20

Figure 3-4. Solar spectral reflectances of three roofing products: (A) metal (zincalume with clear resin), (B) white membrane, and (C) granule-surfaced modified bitumen cap sheet. Also shown is the solar spectral global horizontal irradiance at Earth's surface (black line) assuming clear sky with the sun at zenith, referred to as Air Mass 1 Global Horizontal (AM1GH). Narrowband spectral ranges (blue, green, red, near-IR) for the airborne digital sensor (ADS80/SH82) used to collect the imagery are shaded. 21

Figure 3-5. Assessment of the empirical model for relating broadband reflectances to narrowband reflectances. All values are computed using solar spectral reflectance measurements of the 190 roof samples (Table 3-2). In (a) visible reflectance $V(b_k, g_k, r_k)$ computed using Eq. (7) is compared to V_k calculated from Eq. (1). The corresponding histogram of residuals is shown in (b). χ is the root mean square of the residuals. In (c), solar reflectance (albedo) $S(b_k, g_k, r_k, i_k)$ computed using Eq. (8) is compared to S_k calculated from Eq. (1); the corresponding histogram of residuals is shown in (d). 22

Figure 3-6. Comparison of pyranometer-measured albedos (ground truths) to (uncalibrated) remotely sensed albedos. The equations shown were applied to the

uncalibrated remotely sensed albedos $S(b_k, g_k, r_k, i_k)$ to compute calibrated values S' using Eq. (3). 24

Figure 3-7. A portion of San Jose showing the mean (calibrated) remotely sensed albedo for each rooftop. 25

Figure 4-1. Roof albedos derived from the remotely sensed imagery for the City of Los Angeles. Roof albedos for each building within city boundaries (indicated by the magenta outline) are projected onto a map in (a). A histogram of roof albedos is shown in (b); *N* is the total number of roofs, μ is the mean roof albedo weighted by roof surface area, and σ is the standard deviation of roof albedos also weighted by surface area. Roof-area weighted (dashed) and non-weighted (solid) cumulative distribution functions (CDFs) are shown in (c). The area-weighted CDF (c) represents the cumulative fraction of roof area, whereas the unweighted curve represents cumulative fraction of roofs. 36

Figure 4-2. Similar to Figure 4-1 but for Long Beach. 38

Figure 4-3. Similar to Figure 4-1 but for Bakersfield. 40

Figure 4-4. Similar to Figure 4-1 but for San Francisco. 42

Figure 4-5. Similar to Figure 4-1 but for San Jose. 44

Figure 4-6. Zoomed in area of Los Angeles showing large buildings with both low and high albedo roofs. Note that the color map in this figure is different than Figure 4-1 to highlight variation in high albedo values. 46

Figure 4-7. Statistical investigations for determining the minimum number of building outlines needed to calculate the mean albedo of a city. Monte Carlo techniques were used to randomly select buildings from the ~1.1 million roof albedos in Los Angeles (shown in Figure 4-1). The evolution of roof area weighted mean albedo as number of roofs included in the sample mean increases is shown in (a). The probability distribution functions of simulated sample means of roof albedo for N = 10, 100, 1000, and 5000 are presented in (b). Tabulated values are number of roofs (*N*), grand mean of sample means

($\mu_{S'}$), and weighted standard deviation ($\sigma_{S'}$) of the sample means over 100,000 simulated samples (with replacement) from the population of ~1.1 million roof albedos in Los Angeles. 47

Figure 4-8. Similar to Figure 4-1 but for Sacramento. Maps are not shown due to the limited sample size. 48

Figure 4-9. Similar to Figure 4-1 but for San Diego. Maps are not shown due to the limited sample size. 49

Figure 4-10. Statistical investigations to test the sufficiency of 1000 roof outlines in (a) Sacramento and (b) San Diego. See Figure 4-7a for further explanation. 50

Figure 4-11. Histograms and root-mean-square (RMS) of scaled arithmetic difference for roofs with duplicate albedos. Duplicate values occurred in areas with overlap of flight paths. The number of duplicate values for each city is in Table 4-1. A small fraction of roofs had arithmetic difference greater than the horizontal axis range shown. These roofs were included in the calculation of RMS. 51

Figure 4-12. Fraction of urban roof area comprised of roofs that are (a) smaller and (b) larger than a range of roof area thresholds. Also shown are mean albedos for all roofs (c) smaller and (d) larger than the roof area thresholds. Mean albedos are weighted by roof area. 53

Figure 4-13. Surface albedos accounting for all land cover types used as an input to the meteorological model (WRF). Default albedos derived using only MODIS observations are in (a). Albedos used in the ‘base_case’ and ‘cool_roof’ scenarios are in (b) and (c). The magenta line shows Bakersfield city limits. Black cells southwest of Bakersfield indicate water. 55

Figure 4-14. Mean change in summer (a) and winter (b) air temperature due to cool roofs, computed as ‘cool_roof’ minus ‘base_case’ scenarios. Temperatures are diagnosed as 2 meter air temperature at 15:00 LST. Only changes that are significant at the 95% confidence level are shown. 56

List of Tables

Table 3-1. Sources of shapefiles containing outlines of all buildings within five of the seven cities of focus. Outlines were not available in Sacramento and San Diego..... 15

Table 3-2. Roofing samples for which we measured solar spectral reflectances in the laboratory. 16

Table 3-3. Estimated error ε (accuracy) at 90% confidence interval of the calibrated remotely sensed albedos. ε is shown for each city and for different values of calibrated albedo S'. One-sided confidence intervals are shown because they are asymmetric about the mean; ε^{U} is the upper and ε^{L} the lower interval. The City of Los Angeles and Long Beach are shown together since both are part of the Greater Los Angeles Area..... 17

Table 4-1. Number of roofs, total roof surface area, and mean and standard deviation of roof albedos for each city..... 34

Table 4-2. Properties for roofs with area > 5,000 m^2..... 35

List of Acronyms, Initialisms, and Symbols

AM1GH - air mass one global horizontal

b - narrowband reflectance in the blue (420 – 492 nm)

CEC - California Energy Commission

f - fraction of grid cell

g - narrowband reflectance in the green (533 – 587 nm)

HVAC - heating, ventilation, and air conditioning

i - narrowband reflectance in the near-IR (833 – 920 nm)

I - broadband near-IR reflectance (700 – 2500 nm)

$j(\lambda)$ - solar spectral irradiance

LST - local standard time

MODIS - MODerate resolution Imaging Spectroradiometer

N - number of roofs

NARR - NCEP North American Regional Reanalysis

NDVI - normalized difference vegetation index

r - narrowband reflectance in the red (604 – 664 nm)

R - irradiance weighted band reflectance

RMS - root mean square (also referred to as χ)

RRTMG - Rapid Radiative Transfer Model

S - broadband solar reflectance (300 – 2500 nm)

V - broadband visible reflectance (400 – 700 nm)

WRF - Weather Research and Forecasting model

ε - Error

λ - wavelength

μ - city-wide mean roof albedo

$\rho(\lambda)$ - solar spectral reflectance

σ - city-wide standard deviation of roof albedo

Abstract

Cool roofs reflect sunlight and therefore can reduce cooling energy use in buildings. Further, since roofs cover about 20 – 25% of most cities, widespread deployment of cool roofs could mitigate the urban heat island effect and partially counter urban temperature increases associated with global scale climate change. The magnitude of these potential benefits for a given city depends on the increase in albedo that can be achieved using reflective roofs. Assessing this increase requires knowledge of roof albedo at the city-scale, which until now has been unknown due to a lack of reflectance data with sufficient spatial coverage, spatial resolution, and spectral information. In this work we use multiband aerial imagery to derive the albedos of individual roofs in seven California cities: Los Angeles, Long Beach, San Diego, Bakersfield, Sacramento, San Francisco, and San Jose. The radiometrically calibrated, remotely sensed imagery has high spatial resolution (1 m) and four narrow band reflectances: blue, green, red, and near-infrared. First, we locate roof pixels within GIS building outlines. Next, we use laboratory measurements of the solar spectral reflectances of 190 roofing products to empirically relate solar reflectance (albedo) to reflectances in the four narrow bands; the empirical relationship well predicts albedo as indicated by a low root-mean-square of the residuals of 0.016. Albedos computed from remotely sensed reflectances are calibrated to ground measurements of roof albedo in each city. The error (accuracy) at 90% confidence interval of the calibrated albedos is found to vary by city from 0.00 – 0.01 at low albedo and 0.06 – 0.14 at high albedo.

The fraction of urban area covered by roofs ranged by city from 10 to 25%. City-wide average roof albedo ranged from 0.17 ± 0.08 to 0.20 ± 0.11 (mean ± standard deviation) for five of the cities; values were higher in Sacramento (0.24 ± 0.11) and San Diego (0.29 ± 0.15). Buildings with small roofs were found to constitute a large fraction of city roof area and to have low mean albedos. This suggests that efforts to increase urban albedo through the use of reflective roofs should include small roofs, which are presumably mostly residential. Roof albedos derived for Bakersfield were used in a regional climate model (WRF) to estimate temperature changes attainable by converting the current stock of roofs to “cool” high albedo roofs. It was found that seasonal mean afternoon (15:00 LST) temperatures could be reduced by up to 0.2 °C during both the summer and winter. Changes in precipitation were not significant at the 95% confidence level.

1. Executive Summary

In this report we present a method for deriving the mean albedo of individual roofs in California using aerial imagery. The imagery was acquired on an airplane at high spatial resolution (1 m) in four spectral bands (three in the visible and one in the near-IR) using a radiometrically calibrated sensor. Including the near-IR band is important for quantifying roof albedo since (1) some "cool roofs" have low reflectance in the visible but high reflectance in the near-IR, and (2) about 50% of the energy from the sun is in the near-IR part of the solar spectrum. We have developed methods for (a) identifying building outlines, (b) converting the four narrowband reflectances to solar reflectance (albedo) based on laboratory measurements of solar spectral reflectance for 190 roofing products, and (c) calibrating remotely sensed albedos by comparing to measured albedos of several roofs in each city.

We characterize the albedos of individual roofs for seven cities in California: Los Angeles, Long Beach, Bakersfield, San Francisco, San Jose, Sacramento, and San Diego. In the first five cities we report roof albedos for every building within city boundaries, while for the latter two cities we describe on a statistically representative sample of buildings. Using Monte Carlo simulations we randomly sampled from the population of ~1.1 million roofs in Los Angeles to show that 1000 roofs was sufficient for characterizing the mean albedo of a city.

The mean roof albedo (weighted by roof area) for five of the seven cities was 0.17 ± 0.08 to 0.20 ± 0.11 (Los Angeles, Long Beach, San Francisco, San Jose, Bakersfield). The mean roof albedo was slightly higher in Sacramento (0.24 ± 0.11) and even greater in San Diego (0.29 ± 0.15) (Table 4-1).

California public policy that was implemented in 2005 (CEC 2005) requires that new or retrofitted low slope roofs on non-residential buildings should in many cases have high albedo. Roof albedo results presented here were used to estimate the fraction of these roofs that had high albedo in 2009. Since identifying non-residential buildings with low slope roofs was beyond the scope of this study, buildings with footprint area > 5000 m^2 were used as a proxy. The fraction of this subset of buildings with roof albedo > 0.4 varied by city from 3 to 41%. Limitations of this calculation are in Section 4.3.2.

Buildings with small roofs, which are presumably mostly residential homes, represented a large fraction of total city roof area. For example, roofs with area < 400 m^2 made up about 60 to 70% of total roof area while roofs with area >1000 m^2 made up only about 15 to 25% in Los Angeles, Long Beach, San Jose, and Bakersfield. In these cities, roofs with area < 400 m^2 had low city-wide mean albedos ranging from 0.14 to 0.17. Thus, the majority of roof area was made up of small roofs with low albedo. This suggests that increasing the albedo of small (presumably residential) roofs could be an effective way of increasing urban albedo.

We note that there exist "cool colored" roofs with relatively high albedo that are dark in the visible but have high reflectance in the near-IR part of the spectrum. This design allows the roof to maintain a dark appearance while increasing its albedo. Cool colored

roofing products exist with albedos of up to about 0.40. As a point of comparison, white roofs are available with albedos of about 0.90 (CRRC, 2013).

A regional climate model was used to simulate potential temperature changes attainable by converting the current stock of roofs in Bakersfield to cool roofs. Simulations indicated that average afternoon (15:00 LST) temperatures could be reduced by up to 0.2 °C during both the summer and winter. Statistically significant temperature changes were simulated downwind (southeast) of Bakersfield during summer. Cool roofs did not induce statistically significant changes in precipitation.

Temperature changes modeled in this investigation are smaller than changes predicted by past studies for other cities in California (e.g. Taha 2008b). These discrepancies in temperature change are due in part to differences in study design. First, assumed albedo increases in our investigation were from cool roofs only, while Taha also included contributions from cool walls and pavements. A second difference is that Taha reported temperature changes for a four-day high ozone episode, whereas temperature changes reported here are averaged over 10 model weeks per season (2 weeks per season × 5 years). By averaging over this longer time period we are representing climatic seasonal means instead of a particular meteorological regime. We also note that neither study considered the influence of increased urban vegetation on urban climate.

This project resulted in the creation of shapefiles containing outlines and mean roof albedos for every building in Los Angeles, Long Beach, San Francisco, San Jose, and Bakersfield. For Sacramento and San Diego, these shapefiles were created for a reduced but statistically representative sample of buildings (N~1000).

2. Introduction

Roofs cover the top of buildings, separating the atmosphere and the indoor environment. The solar reflectance ("albedo") of a rooftop is the fraction of incident solar energy that is reflected. Sunlight that is not reflected is instead absorbed by the roof; this energy is then transferred to the interior of the building and to the atmosphere. Dark roofs can have albedos as low as 0.05, meaning that they can absorb up to 95% of incident sunlight. Clean bright white roofs can have albedos above 0.90 (CRRC 2013), reflecting nearly all incident sunlight.

Monitoring studies have shown that replacing a dark roof with a white roof can decrease heat flows into the conditioned space, and lower cooling energy use. In many cases, cooling energy use reductions of 10 – 20% have been observed (Parker et al. 1995; Akbari et al. 1997; Parker et al. 1998; Akbari et al. 2001; Konopacki and Akbari 2001; Akbari 2003; Akbari et al. 2005). The cooling energy savings attainable for a particular building depends on its construction, roof and attic insulation, shade cover, and climate. In some situations, such as when roofs are thermally decoupled from the conditioned space, reflective roofs can have negligible effect on energy use (Ban-Weiss et al. 2013). Recognizing the potential energy and cost savings of white roofs, in October 2005 the California Energy Commission added a requirement to its Title 24 Building Energy Efficiency Standards (CEC 2005) that new or retrofitted low-sloped roofs on commercial buildings should in many cases be white. Later updates to these standards added roof reflectance requirements for low-rise residential buildings in certain climate zones (CEC 2008). Appendix B provides a brief summary of cool roof policies in California. When the costs of white and dark roofs are approximately the same, reductions in energy costs translate directly to money saved. Note that while reflective roofs can increase heating energy use requirements in the winter, summer cooling cost savings in most of California's climate zones far outweigh this winter heating cost penalty (Levinson and Akbari 2010).

Solar reflective roofs transfer less heat to the atmosphere than dark roofs. In most cases this reduced heat flow lowers surrounding air temperatures. For example, an observational study (Campra et al. 2008) showed that from 1983 – 2006, a region of southeastern Spain experienced temperature decreases of about 0.3 °C / decade as greenhouses with high albedo roofs were deployed. Since roofs on average comprise about 20 – 25% of surface areas in North American cities (Akbari et al. 1999; Akbari and Rose 2001a; Akbari and Rose 2001b; Akbari et al. 2003; Rose et al. 2003; Akbari and Rose 2008), large-scale deployment of white roofs has been suggested as a measure to mitigate the urban heat island effect (Taha et al. 1998; Akbari et al. 1990; Akbari et al. 1992; Rosenfeld et al. 1995). Similarly, reflective roofs may lessen urban temperature increases associated with global scale climate change. Various mesoscale climate modeling studies have simulated the climate effects of hypothetical increases in urban albedo. For example, simulations reported by Taha (2008a) found 1 – 2 °C decreases in peak urban temperatures at six locations in California. Other studies have shown comparable temperature reductions in other regions (Synnefa et al. 2008; Taha 2008b; Lynn et al. 2009; Zhou and Shepherd 2009). We note that one study showed that in some situations urban air temperatures can rise with increased urban albedo (Taha 2008c); this

study hypothesized that the modeled temperature increase in Houston, Texas was due to reduction of the atmospheric mixing height.

Other modeling studies have investigated the effect of increasing urban albedo at the national scale (Millstein and Menon 2011) and global scale (Menon et al. 2010; Oleson et al. 2010; Jacobson and Ten Hoeve 2012; Akbari et al. 2012). Millstein and Menon (2011) used a regional climate model to show that adopting cool roofs and pavements in urban areas of the United States could reduce afternoon summertime temperatures in urban locations by 0.1 – 0.5 °C. A study using a global climate model (Oleson et al. 2010) demonstrated that reflective surfaces could decrease the annual mean urban heat island effect[1] to 0.8 °C from 1.2 °C.

While reflective surfaces have been modeled in most situations to reduce urban temperatures, their effects on the hydrological cycle also warrants investigation. One mesoscale climate modeling study (Georgescu et al. 2012) has suggested that reflective surfaces may reduce precipitation around Phoenix, Arizona. Since Phoenix has unique desert meteorology with most of its precipitation arriving with late-summer monsoon thunderstorms, this result may not hold in other regions.

Determining realistic estimates of the potential for increasing roof albedo at the city scale requires detailed understanding of the current stock of roofs. Currently there are no estimates of the mean urban roof albedos. There are at least five challenges associated with quantifying roof albedo at the city scale: spatial coverage, spatial resolution, spectral coverage, radiometric calibration, and cost. For example, roof albedo can be accurately measured at the rooftop by using a pyranometer to measure incident and reflected sunlight (ASTM 2006). However, measuring a sample large enough to statistically represent the roofs of a city is logistically prohibitive. Remote sensing can rapidly characterize large geographic areas. For example, there exist freely available surface albedo datasets derived from satellite sensors like MODIS (Schaaf et al. 2002; Schaaf 2004). However, its spatial resolution of 1 minute (2 km at equator, <1 km at pole) is too low to distinguish various urban surface types such as roofs. Imagery from commercial satellites (e.g., GeoEye, IKONOS) offers spatial resolutions of about 0.5 m and spectral information in the visible and near-infrared (near-IR). While the spatial resolution and spectral coverage may be sufficient to distinguish roofs and compute roof albedo, purchasing these imagery for entire cities would be costly. Another option is aerial imagery, which is often acquired from aircraft. Since these aircraft are generally nearer to the ground than satellites, the captured imagery is at higher spatial resolution. While aerial imagery can sometimes provide multiband information in the visible and near-IR, it is almost always acquired for generating photographs and therefore does not provide the calibrated radiance data needed for scientific analysis.

In this report we develop a novel method for using radiometrically calibrated aerial imagery to derive roof albedos for seven cities in California: Los Angeles, Long Beach, San Diego, Bakersfield, Sacramento, San Francisco, and San Jose. The aerial imagery has

[1] The urban heat island effect was defined by Oleson et al. (2010) as the difference (urban – non-urban) in 2-m air temperature between urban and non-urban portions of model grid cells.

high spatial resolution (1 m) and includes reflectances in four narrow spectral bands: three in the visible (blue, green, and red), and one in the near-infrared. In Section 3, we present methods for calculating roof albedo from remotely sensed reflectances, and show sample results. Section 4 reports roof albedos in each of the seven California cities of interest. It also provides further analyses and applications using the albedo dataset. Applications include use of roof albedos in a regional climate model to estimate temperature decreases attainable by converting the current stock of roofs to solar reflective cool roofs. Section 5 provides a summary and conclusions. This work is the first of its kind to quantify the albedos of individual roofs at the scale of entire cities.

3. Developing the Methods

3.1. Methods

In this section we describe the methods developed to derive the albedos of roofs in seven California cities: Los Angeles, Long Beach, San Diego, Bakersfield, Sacramento, San Francisco, and San Jose. Figure 3-1 diagrams the approach. Reflectances in narrow bands denoted blue, green, red, and near-IR were obtained from high spatial resolution (1 m) imagery acquired using airplanes during summer 2009. We refer to the data collected using the airplane as "remotely sensed." Pixels containing roofs were then extracted from the imagery. Roof pixels were identified using GIS building outline datasets for entire cities where available. When building outline datasets were not available, manual tracing of buildings was performed. Laboratory measurements of the solar spectral reflectances of 190 roofing products were used to empirically relate solar reflectance (albedo) to reflectances in the four narrow bands. Albedos computed from remotely sensed reflectances were calibrated to ground measurements of roof albedo in each city. Pixels within each roof boundary were then averaged to calculate the mean albedo of each roof. Each step is now described in more detail.

3.1.1 Data source

The aerial imagery was originally acquired for the National Agriculture Imagery Program (NAIP), which is administered by the US Department of Agriculture (USDA). NAIP annually acquires aerial imagery during the agricultural growing season (late spring to early summer) in the continental United States. One of the main goals of NAIP is to provide digital ortho photography to government agencies and the public. While this program is focused on agriculture, imagery is generally acquired for entire states including urban areas. NAIP has strict requirements to ensure high image quality. For example, to minimize shadows, flights must occur when the sun is at least 30 degrees above the horizon. In practice, almost all imagery is collected when the sun is at least 60 degrees above the horizon. Flights must acquire imagery on clear days without cloud cover (NAIP 2013).

NAIP imagery is available for the entire state of California at 1 m spatial resolution in years 2005, 2009, 2010, and 2012 (NAIP 2013). NAIP contracts different companies to acquire imagery each year. As such, various imagery acquisition systems have been used. In 2009, imagery for California was collected by North West Group (Calgary, Alberta, Canada) using a Leica ADS80/SH82 airborne digital sensor (Leica 2013). This sensor is more than a high-speed digital camera for photography. It utilizes arrays of digital charge-coupled devices that sense light in four narrow spectral bands (blue, 420 – 492 nm; green, 533 – 587 nm; red, 604 – 664 nm; and near-IR, 833 – 920 nm). The arrays of detectors are arranged perpendicular to the flight direction in a "push broom" configuration. Each detector is radiometrically calibrated in the laboratory to accurately measure radiance in its spectral band. Thus, the sensor accurately measures multi-spectral radiance, similar to that acquired by sensors on satellites for scientific applications. In this way, the imagery collected by the sensor has the potential to be used as a scientific remote sensing data set, rather than simply as photographs. NAIP imagery is publically

available as either “digital ortho quarter quad tiles” (DOQQs) or “compressed county mosaics” (CCM); both options include imagery compression, a variety of color adjustments, and other post-processing required by NAIP (NAIP 2013). This post-processing improves the overall appearance and usability of the imagery, but destroys the radiometric calibration, which is important for the purposes of this study. Therefore, we acquired directly from NAIP’s vendor for 2009 (North West Group) the radiometrically calibrated source data for images within our cities of interest. The field of view of the sensor resulted in image footprints that are 12 km wide (perpendicular to flight direction), and of varying length depending on flight paths. The mean altitude of the flights was about 9 km above ground level. Each flight strip has 15% overlap with the adjacent flight strip; thus, about 30% of the area for each city has duplicate imagery.

The near-IR contains approximately 50% of the energy from the sun (Levinson et al. 2010). Some “cool roofs” have low reflectance in the visible but high reflectance in the near-IR, allowing the roof to remain dark while increasing its albedo (Levinson et al. 2007). Thus, having information about reflectance in both the visible and near-IR spectra improves estimates of roof albedo.

3.1.2 Correcting for the atmosphere and bidirectional reflectance distribution

Since we are interested in reflectance at Earth’s surface, the radiance measurements at the sensor (on the airplane) needed to be corrected for atmospheric scattering and the bidirectional reflectance distribution function (BRDF). Techniques have been previously developed and described at length elsewhere, so we provide only a brief description here. Atmospheric gases and particles can influence the perceived “at-sensor” radiance through multiple pathways (Downey et al. 2010). For example, sunlight can be scattered into the sensor by atmospheric constituents. The atmospheric correction attempts to isolate the radiance that originates from the Earth surface. The correction used in this work was a modified Song-Lu-Wesley method (Downey et al. 2010). Past studies have validated the atmospheric correction by comparing to ground reflectance measurements (Beisl and Adiguezel 2010; Markelin et al. 2010) and found agreement to within 10%. The BRDF correction, based on a modified Walthall method (Beisl et al. 2008, Downey et al. 2010), was implemented to remove an artifact caused by the fact that reflectance is a function of viewing angle, and therefore depends on distance from the center of the flight path. Since flights for NAIP are always in the north-south direction, the BRDF correction minimizes spurious east-west gradients in reflectance (i.e., perpendicular to the flight direction). The correction uses statistics of only land pixels and therefore specular reflectance from water did not influence results (Downey et al. 2010). The corrected imagery reports values of surface reflectance for each of the four narrow bands in each 1 m pixel; we refer to these as the remotely sensed blue, green, red, and near-infrared reflectances. Figure 3-2 shows example imagery for the four narrow bands in a portion of San Jose, California. Low reflectance pixels in each narrow band are dark, and high reflectance pixels are white. (Note that the line of trees on the right side of the image shows higher reflectance in near-IR than in the red, a characteristic of light reflection from leafs (Slatton et al. 2001).)

The remainder of the method sections describe our derivation of roof albedo from the imagery (Figure 3-2).

3.1.3 Extracting roof pixels from the imagery

Next we identify in the imagery pixels containing roofs. For five of the seven cities of interest (Los Angeles, Long Beach, Bakersfield, San Francisco, and San Jose), shapefiles containing outlines for every building within the city were acquired from local governments (Table 3-1). Example building outlines projected onto a red-green-blue (RGB) composite of the aerial imagery in San Jose are shown in Figure 3-3a. The building outlines include detailed features of each building, as can be better observed when projected onto higher spatial resolution (but not radiometrically calibrated) imagery from United States Geological Survey (Figure 3-3b). In our analysis we assume that building outlines and roof outlines are colocated.

In the two cities for which we could not acquire building outlines (Sacramento and San Diego), we manually traced the edges of buildings in the imagery using ESRI ArcMap 10.0. Manually tracing perfect outlines provided difficult. We therefore intentionally traced outlines that were slightly within the actual building borders, ensuring that non-roof pixels were not included within the boundaries. Manually tracing every building was not feasible, so we traced a small but statistically representative sample of buildings within each of these two cities. To determine the number of buildings needed to properly characterize the mean roof albedo of a city, we performed a Monte Carlo statistical investigation using the population of albedo values computed for Los Angeles. As shown in Section 4.2.2.1, 1000 roof outlines was found to be sufficient. Hundreds of 300 x 300 m^2 quadrats (small, typically rectangular study regions) were generated in random locations within city boundaries; all roofs within the borders of the quadrats were traced until the minimum number of outlines (N=1000) was met. An example of manually traced outlines within a quadrat in Sacramento is shown in Figure 3-3c.

3.1.4 Relating albedo to narrowband reflectances

To quantify the albedo of individual roofs, we need a method to relate albedo to the four (narrowband) remotely sensed reflectances. We began by computing the solar, visible, and narrowband (blue, green, red, and near-IR) reflectances of each of 190 roofing products from laboratory measurements of solar spectral reflectance. Included in the 190 samples were all widely used roofing types in California for both commercial and residential buildings (Table 3-2). Samples were new and mostly acquired from various roofing supply stores in the San Francisco Bay area. Clay tile samples were provided by MCA Superior Clay Roofing Tiles. While use of roofing materials that had been aged outdoors was desired, it was infeasible to collect soiled roofing materials. Solar spectral reflectance was measured using a PerkinElmer Lambda 900 UV/Vis/NIR spectrophotometer equipped with a 150-mm Labsphere integrating sphere. Spectral reflectances were measured from 300 to 2500 nm in 5 nm steps.

Figure 3-4 shows the solar spectral reflectance, $\rho(\lambda)$, of several roofing products, as well as the solar spectral irradiance, $j(\lambda)$, used to compute band reflectances. This air mass

one global horizontal (AM1GH) terrestrial irradiance assumes a clear sky and the sun at zenith, and is suited to characterizing roof albedo (Levinson et al. 2010). Irradiance-weighted band reflectance R over each range of interest was calculated as

$$R = \frac{\int_{\text{range}} j(\lambda)\rho(\lambda)d\lambda}{\int_{\text{range}} j(\lambda)d\lambda}. \quad (1)$$

We computed four narrowband reflectances—blue, b (420 – 492 nm); green, g (533 – 587 nm); red, r (604 – 664 nm); and near-IR, i (833 – 920 nm)—and three broadband reflectances: visible, V (400 – 700 nm), near-IR, I (700 – 2500 nm), and solar, S (300 – 2500 nm). (Narrowband spectral ranges correspond to those of the remote sensor. Lowercase symbols represent narrowband reflectances and uppercase symbols represent broadband reflectances.) Note that while the narrow blue, green, and red spectra collectively span most of the visible spectrum, the narrow near-infrared spectrum used to compute i spans less than 5% of the full near-infrared spectrum (700 – 2500 nm) (Figure 3-4). Hence, we expect (b, g, r) to predict V more accurately than (b, g, r, i) can predict S.

Using the aforementioned laboratory measurements we developed empirical relationships between broadband and narrowband reflectances using multivariate regression. We first modeled $V = V(b, g, r)$ to test the method, then modeled $S = S(b, g, r, i)$. This technique is similar to past work that predicted albedo from narrowband reflectances measured by sensors on satellites (Liang 2000; Liang et al. 2002). These studies focused on developing universal conversion formulas that worked for multiple land cover types, with a focus on natural vegetative surfaces. Our task is somewhat different since we focus on one man-made surface type (roofs). Acquiring and measuring spectral reflectances of a large sample of roofing products likely presented less of a challenge than doing so for a wide range of natural surfaces.

3.1.5 Calibrating remotely sensed albedos using ground truths

To calibrate the remotely sensed albedos, we measured the albedos of several roofs in each city, and then evaluated $S(b, g, r, i)$ for these roofs using remotely sensed b, g, r, and i. Measured albedos were obtained using one of two methods. In the first, we identified buildings that had new roofs installed within six months prior to the flights. The make and model of the new roof was known, allowing us to obtain its albedo from an online database (CRRC 2013). In the second, we measured rooftop albedos with a pyranometer. The pyranometer measurements were performed in July 2012 in San Jose and Los Angeles, and in September 2012 in San Francisco and Davis (near Sacramento). Since these measurements were taken about three years after the imagery was acquired via airplane, the second method was implemented only for roofs with low measured albedos (S < 0.4); as shown in Sleiman et al. (2011), aging (i.e., weathering and soiling) had a small effect on the albedo of such roofs in this range. White roofing products can

show marked decreases in albedo after three years (Sleiman et al. 2011) and were therefore not included in this second method.

Method 1 (applied to all roofs). Several roof manufacturers and vendors identified the make and model of roofs installed in each city no more than six months prior to each flight. The initial solar reflectance of each installed roof was then obtained from the Rated Products Directory of the Cool Roof Rating Council (CRRC 2013). Corresponding remotely sensed albedos were then quantified by randomly sampling 10 pixels within the roof boundary. Only pixels with visible roofing material were included; HVAC equipment, solar photovoltaics, skylights, and other features were excluded. In total, 31 buildings with known installation dates and roofing product types were used.

Method 2 (applied only to roofs with low measured albedo). We measured the albedo of roofs on 10 buildings in (or very near) four of the seven cities with a Kipp & Zonen CMA6 first-class albedometer, which integrates back-to-back a pair of Kipp & Zonen CMP6 first-class pyranometers. Albedos were measured following ASTM Standard E1918-06, "Standard Test Method for Measuring the Solar Reflectance of Horizontal and Low-Sloped Surfaces in the Field" (ASTM 2006). Three consecutive albedo measurements were performed at each of three locations on each roof, for a total of nine measurements per roof. The mean albedo was calculated by averaging these nine measurements. Corresponding remotely sensed albedos were extracted by identifying each measurement location in the imagery; the mean value of pixels within a 3 m radius was calculated to approximate the field of view of the pyranometer. This was done for each of the three measurement locations per roof. The three resulting albedos were then averaged and compared to the measurement-derived mean albedo for each roof.

We were unable to obtain measurements for low albedo roofs in Bakersfield using either Method 1 or 2. Instead, we obtained from Bakersfield Public Works records of asphalt concrete pavement installations. Two roads were paved within one year prior to the flights; installations were 3 weeks and 8 months prior to the flights, respectively. Associated albedos were assumed to be 0.05 and 0.07, respectively, derived from measurements of the post-installation time evolution of asphalt pavement albedo (unpublished). Corresponding remotely sensed albedos were obtained using the random sampling technique described above for Method 1.

Measured albedo, S_{measured}, was regressed to remotely sensed albedo, $S(b,g,r,i)$, using a power law relationship of the form

$$S_{\text{measured}} = a_c S^{p_c} \qquad (2)$$

This was done separately for each city to determine parameters a_c and p_c, where subscript *c* indexes the seven cities. These power law parameters were then used to determine the calibrated remotely sensed (pixel level) albedo S' in each city as

$$S' = a_c S^{p_c} \qquad (3)$$

where the prime indicates "calibrated." The error ε (accuracy) of the remotely sensed albedos (S') in each city was then estimated using the standard errors of the power law parameters. Upper and lower-bound estimates of the coefficients were derived as mean value ±90% confidence interval. One-sided confidence intervals above (ε^{U}) and below (ε^{L}) the mean were then calculated as a function of calibrated albedo as

$$\varepsilon^{\mathrm{U}}(S') = a_c^{\mathrm{U}} S^{p_c^{\mathrm{U}}} - S' \qquad (4)$$

$$\varepsilon^{\mathrm{L}}(S') = S' - a_c^{\mathrm{L}} S^{p_c^{\mathrm{L}}} \qquad (5)$$

where superscripts U and L correspond to upper- and lower-bound parameter estimates. These error estimates indicate the accuracy with which calibrated albedos are calculated from uncalibrated remotely sensed values. Note that we present one-sided confidence intervals because the power law form of Eq. (3) makes ε asymmetric about S'.

White roofs are commonly single-ply (plastic) membranes or elastomeric coatings, both of which are very smooth and glossy when new. Reflection from these materials can therefore include a non-negligible specular component at high angles of sunlight incidence (e.g., see Levinson et al. 2010). Since white roofs are almost always low-slope and flights occurred with the sun at least 60° above the horizon, we expect in most cases that the specular component of reflection will be negligible. However, some commercial roofs can be "wavy" and have areas with high pitch, making the incidence angle large and introducing a non-negligible specular reflection. Such instances were seen in the remotely sensed data as widely varying pixel-level roof albedos within the boundaries of a roof, and were more likely to occur near the edges of flight strips. To ensure that roofs used for calibration had negligible specular reflection reaching the aerial sensor, we omitted buildings that (a) were near the flight strip edges, and (b) contained pixel-level albedos within the roof boundary that varied by more than 0.1.

3.1.6 Mean albedo for each roof

Mean albedos for each roof were calculated by averaging S' within each building outline. Some non-roofing materials were included since roofs can house HVAC equipment, skylights, solar photovoltaics, and other features. While we expect such equipment to minimally affect the mean roof albedo for each city, it can strongly affect the albedo of individual roofs.

3.1.7 Precision of the remotely sensed albedos

As was mentioned in Section 3.1.1, about 30% of each city has overlapping imagery and therefore two values of remotely sensed roof albedo. For each city, duplicates were used to determine the precision error calculated as the scaled arithmetic difference,

$$\text{Scaled arithmetic difference} = \frac{(S_2' - S_1')}{\sqrt{2}} \qquad (6)$$

where subscripts 1 and 2 describe each duplicate value. Note that there is imprecision in each value S_1' and S_2'; since these imprecisions add quadratically, we divide by $\sqrt{2}$ in Eq. (6) to determine the precision of one measurement (Hyslop and White 2009).

3.2. Results

3.2.1 Obtaining solar reflectance (albedo) from remotely sensed (narrowband) reflectances

We modeled $V = V(b, g, r)$ using the simple linear form

$$V_k = c_\mathrm{b} b_k + c_\mathrm{g} g_k + c_\mathrm{r} r_k . \qquad (7)$$

Here V_k, b_k, g_k, and r_k are band reflectances computed from Eq. (1); each *c* is a fitted coefficient; and subscript k indexes the 190 roofing samples. This linear model with $c_\mathrm{b} = 0.37$, $c_\mathrm{g} = 0.30$, and $c_\mathrm{r} = 0.31$ predicts V with a coefficient of determination R^2 = 0.99. Figure 3-5a evaluates the empirical model by comparing $V(b_k, g_k, r_k)$ to V_k. The minimal deviation of points from the one-to-one line indicates that the linear model well predicts V. A histogram of residuals (Figure 3-5b) shows that the linear model can predict V to within 0.02; the root mean square (RMS) error χ is 0.003. Adding higher order terms and/or cross products to Eq. (7) did not improve the fit.

Next we attempted to quantify albedo as

$$S_k = c_\mathrm{b} b_k + c_\mathrm{g} g_k + c_\mathrm{r} r_k + c_\mathrm{i} i_k . \qquad (8)$$

The linear model with $c_\mathrm{b} = 0.17$, $c_\mathrm{g} = -0.13$, $c_\mathrm{r} = 0.33$, and $c_\mathrm{i} = 0.54$ predicts S with R^2 = 0.99. Figure 3-5c evaluates the empirical model by comparing $S(b_k, g_k, r_k, i_k)$ to S_k. Again, there is minimal deviation from the one-to-one line, showing that the linear model well predicts S. More complicated variants to Eq. (8) were evaluated, this time including a term equal to the normalized difference vegetation index (NDVI).[2] The more complex models were found to be no better than the simple linear equation (Eq. (8)). A histogram of residuals is shown in Figure 3-5d. The linear model can predict S with an RMS error of 0.016.

[2] NDVI is a metric that is often used to determine whether pixels contain live vegetation, and is calculated as $(I - V)/(I + V)$. Live vegetation characteristically has higher near-IR reflectance than visible reflectance and therefore NDVI > 0. The use of NDVI in this study was an attempt to identify cool roofs with low reflectance in the visible but high reflectance in the near-infrared. While the metric successfully identified cool colored roofs, adding it as a term to Eq. (8) did not improved the empirical model.

The largest outlier is a metal roofing sample (zincalume with clear resin finish) in which $S(b_k, g_k, r_k, i_k)$ underpredicts S_k by 0.10. Figure 3-4 shows the spectral reflectance of this outlier. It can be seen that the narrowband near-IR spectral range does not capture the increased reflectance at $\lambda > 1000\,\text{nm}$; thus, i (833 – 920 nm) underpredicts broadband near-IR reflectance (700 – 2500 nm). A roofing product with strongly varying spectral reflectance in the near-IR may not always be well characterized by the narrowband near-IR reflectance i.

That albedo can be well characterized using a linear combination of narrowband reflectances is consistent with results from Liang (2000) and Liang et al. (2002). They derived empirical relationships between albedo and narrowband reflectances for satellite sensors (e.g., ASTER, MODIS, ETM+, MISR) and nearly all derived relationships were linear.

3.2.2 Calibrating remotely sensed albedos using ground truths

Figure 3-6 shows measured versus remotely sensed (uncalibrated) albedos for the buildings that served as ground truths. Results for the City of Los Angeles and Long Beach are shown together since they are both part of the Greater Los Angeles Area. For low measured albedo (S < 0.4) most remotely sensed values are near measured values with a maximum discrepancy of 0.09. Remotely sensed albedos are consistently lower than measured values. For high measured albedo ($S \geq 0.4$), the discrepancy is larger with remotely sensed values up to about 50% lower than measured values. To derive remotely sensed (calibrated) albedos, the equations shown in Figure 3-6 were applied to the uncalibrated values using Eq. (3) in each city.

Table 3-3 shows an estimate of the error (accuracy) at 90% confidence interval of the calibrated remotely sensed albedos. Error was calculated using Eqs. (4) and (5). Low albedo values are quite accurate, while high albedo values are generally less accurate. Note that the error for high albedo values is smaller in San Jose than in the other cities because we had a relatively high number (N=8) of high albedo measurements, all of which had consistent remotely sensed values. The reported errors represent the estimated accuracy associated with the mean value for a given roof. However, the relatively large error for high albedo roofs is unlikely to markedly influence the mean roof albedo for each city if high albedo roofs comprise a relatively small fraction of total urban roof area. There may exist high albedo roofs at the flight strip edges that have errors larger than reported (i.e., outside the 90% confidence intervals) because of specular reflectance. These outliers would most commonly have newly installed high albedo roofs with "curvy" roof shapes. The curves in the roof would mean that certain areas have high incidence angles and therefore significant specular reflectance (see Section 3.1.5).

3.2.3 Maps of roof albedo

Figure 3-7 shows a zoomed in area of San Jose with the mean value of calibrated albedo S' for each roof. As expected in California due to Title-24 Building Energy Efficiency Standards (CEC 2005), some commercial buildings with large flat roofs have high

albedo. Homes with pitched roofs usually have low albedo roofs. Section 4 shows city-wide results for all seven cities and provides further analysis.

3.2.4 Discussion and Conclusions

In this chapter we have presented a method for deriving the mean albedo of individual roofs in California using aerial imagery. The imagery was acquired on an airplane at high spatial resolution (1 m) in four spectral bands (three in the visible and one in the near-IR) using a radiometrically calibrated sensor. Including the near-IR band is important for quantifying roof albedo since (1) some "cool roofs" have low reflectance in the visible but high reflectance in the near-IR, and (2) about 50% of the energy from the sun is in the near-IR part of the solar spectrum. We have developed methods for (a) identifying building outlines, (b) converting the four narrowband reflectances to solar reflectance (albedo) based on laboratory measurements of solar spectral reflectance for 190 roofing products, and (c) calibrating remotely sensed albedos by comparing to measured albedos of several roofs in each city.

In Section 4 we present city-wide albedo results for our seven California cities of interest, report results of the precision analysis based on duplicate albedo values for roofs in flight overlap areas, and provide additional analyses based on the city-wide results. We also use the roof albedo results for Bakersfield as an input to a regional climate model to predict the summer and winter temperature and precipitation changes that could result from converting the current stock of roofs to cool roofs.

Table 3-1. Sources of shapefiles containing outlines of all buildings within five of the seven cities of focus. Outlines were not available in Sacramento and San Diego.

City	**Source**
San Jose	City of San Jose (2011)
San Francisco	City and County of San Francisco (2011)
Bakersfield	City of Bakersfield (2011)
City of Los Angeles	Los Angeles Region Imagery Acquisition Consortium 3 (2011)
Long Beach	Los Angeles Region Imagery Acquisition Consortium 3 (2011)

Table 3-2. Roofing samples for which we measured solar spectral reflectances in the laboratory.

Roofing product type	**Number of samples**
Asphalt shingle	75
Concrete tile	25
Clay tile	36
Metal roofing	5
Single-ply membrane	30
Modified bitumen cap sheet	14
Field-applied coating	5
Total	**190**

Table 3-3. Estimated error ε (accuracy) at 90% confidence interval of the calibrated remotely sensed albedos. ε is shown for each city and for different values of calibrated albedo S'. One-sided confidence intervals are shown because they are asymmetric about the mean; ε^{U} is the upper and ε^{L} the lower interval. The City of Los Angeles and Long Beach are shown together since both are part of the Greater Los Angeles Area.

	Error											
Albedo	Los Angeles / Long Beach		Sacramento		San Jose		San Francisco		San Diego		Bakersfield	
	ε^{U}	ε^{L}	ε^{U}	ε^{L}	ε^{U}	ε^{L}	ε^{U}	ε^{L}	ε^{U}	ε^{L}	ε^{U}	ε^{L}
0.1	0.00	0.00	0.00	0.00	0.00	0.00	0.00	0.00	0.01	0.01	0.00	0.00
0.2	0.01	0.01	0.02	0.02	0.00	0.00	0.01	0.01	0.00	0.00	0.00	0.00
0.3	0.01	0.02	0.03	0.03	0.00	0.00	0.02	0.02	0.00	0.00	0.01	0.01
0.4	0.02	0.02	0.04	0.05	0.01	0.01	0.03	0.03	0.01	0.01	0.02	0.02
0.5	0.03	0.03	0.06	0.07	0.02	0.02	0.04	0.04	0.02	0.02	0.03	0.03
0.6	0.04	0.05	0.07	0.08	0.02	0.03	0.05	0.05	0.03	0.03	0.04	0.04
0.7	0.05	0.06	0.09	0.10	0.03	0.04	0.06	0.07	0.04	0.04	0.05	0.05
0.8	0.06	0.07	0.10	0.12	0.04	0.05	0.07	0.08	0.05	0.05	0.06	0.06
0.9	0.08	0.08	0.12	0.14	0.06	0.06	0.09	0.10	0.06	0.07	0.07	0.08

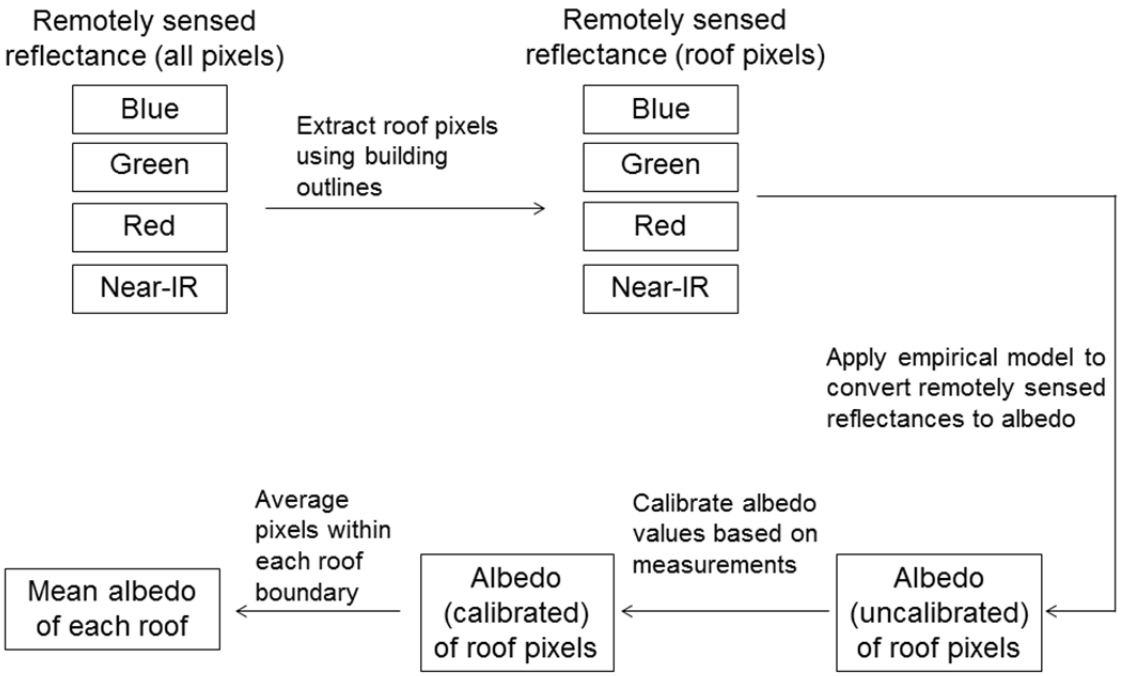

Figure 3-1. Schematic of our approach for deriving the mean albedo of individual roofs from the aerial imagery.

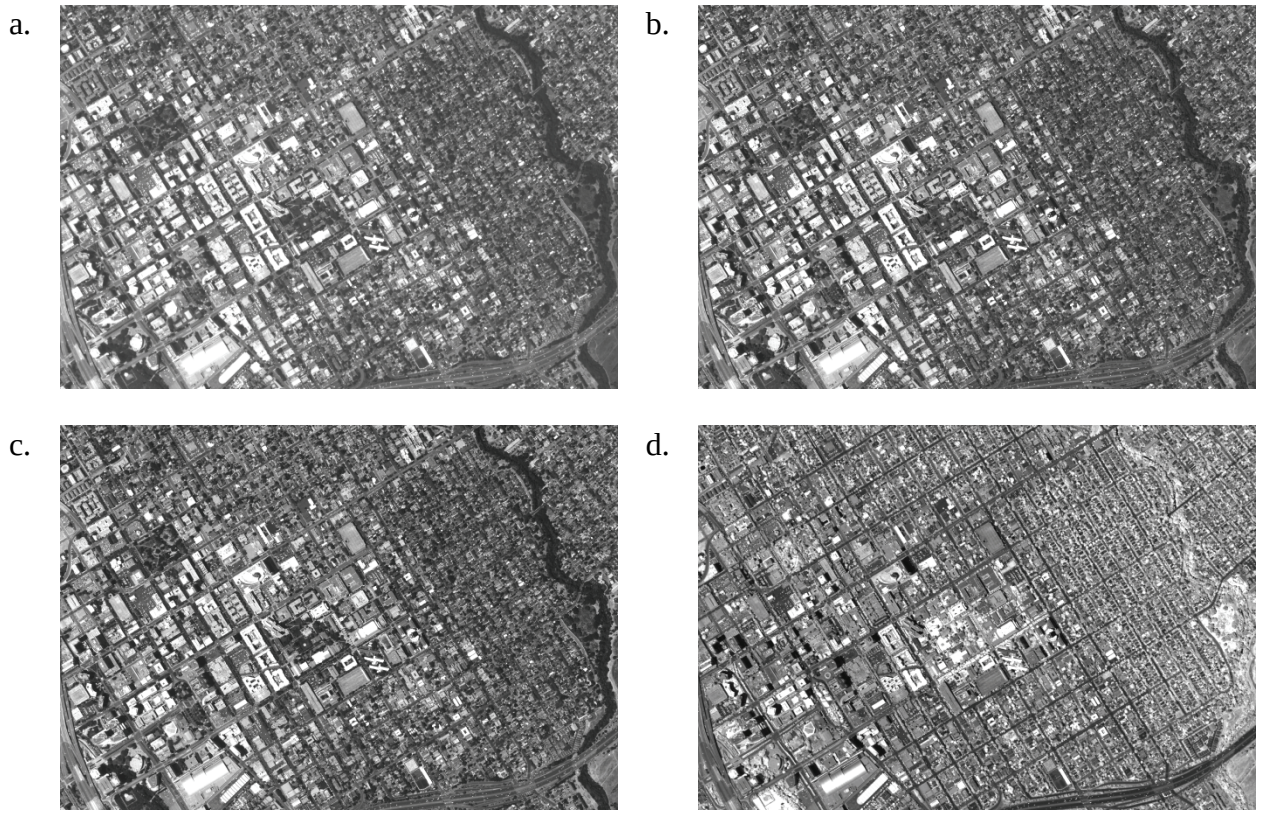

Figure 3-2. Examples of the 1 m resolution remotely sensed imagery for a portion of San Jose, California, showing reflectance in four narrow bands: (a) blue (420 – 492 nm), (b) green (533 – 587 nm), (c) red (604 – 664 nm), and (d) near-IR (833 – 920 nm).

a

b

c

Figure 3-3. Example building outlines. Outlines provided by the City of San Jose are shown in (a) and (b). Manually traced outlines in Sacramento are in (c). In (a) and (c) the underlying imagery is an RGB composite of the aerial imagery described in this report. In (b) the underlying imagery (source = United States Geological Survey) is higher spatial resolution to help distinguish fine-scale features; this imagery but not radiometerically calibrated.

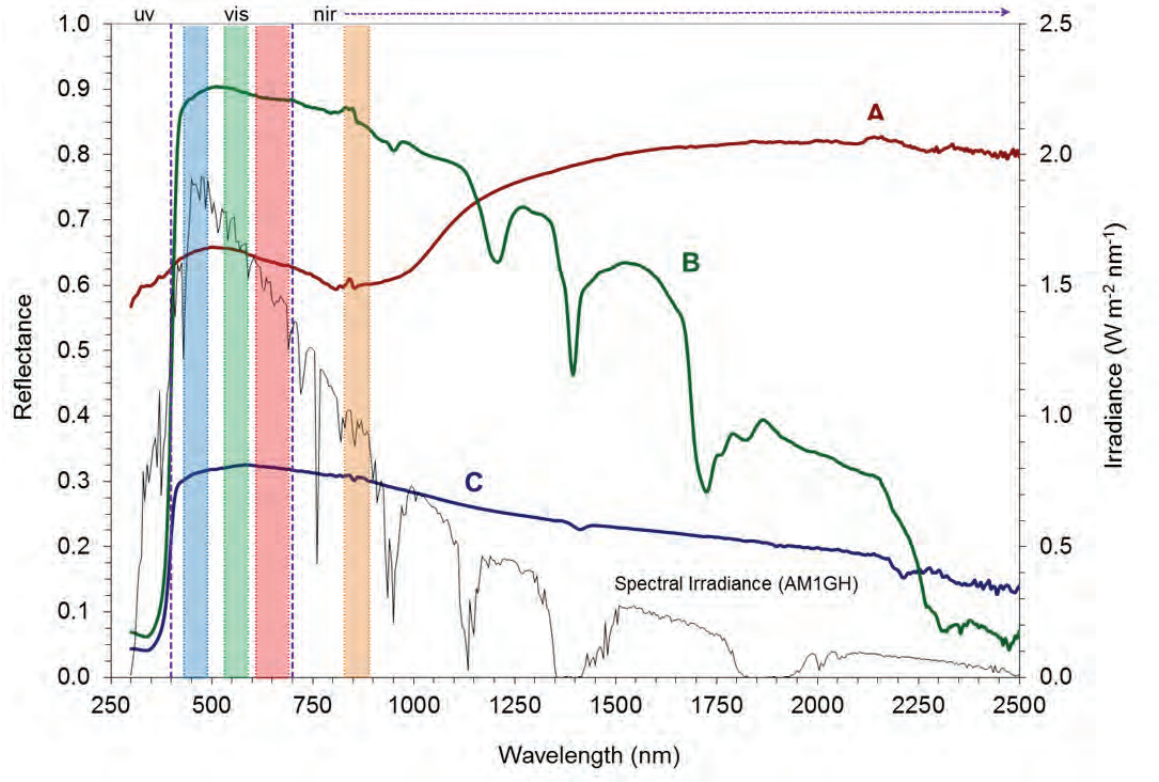

A. Metal roof

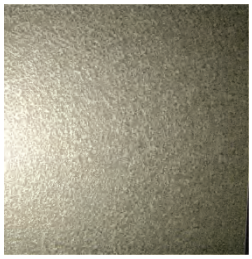

B. White membrane

C. Cap sheet

Figure 3-4. Solar spectral reflectances of three roofing products: (A) metal (zincalume with clear resin), (B) white membrane, and (C) granule-surfaced modified bitumen cap sheet. Also shown is the solar spectral global horizontal irradiance at Earth's surface (black line) assuming clear sky with the sun at zenith, referred to as Air Mass 1 Global Horizontal (AM1GH). Narrowband spectral ranges (blue, green, red, near-IR) for the airborne digital sensor (ADS80/SH82) used to collect the imagery are shaded.

a.

b.

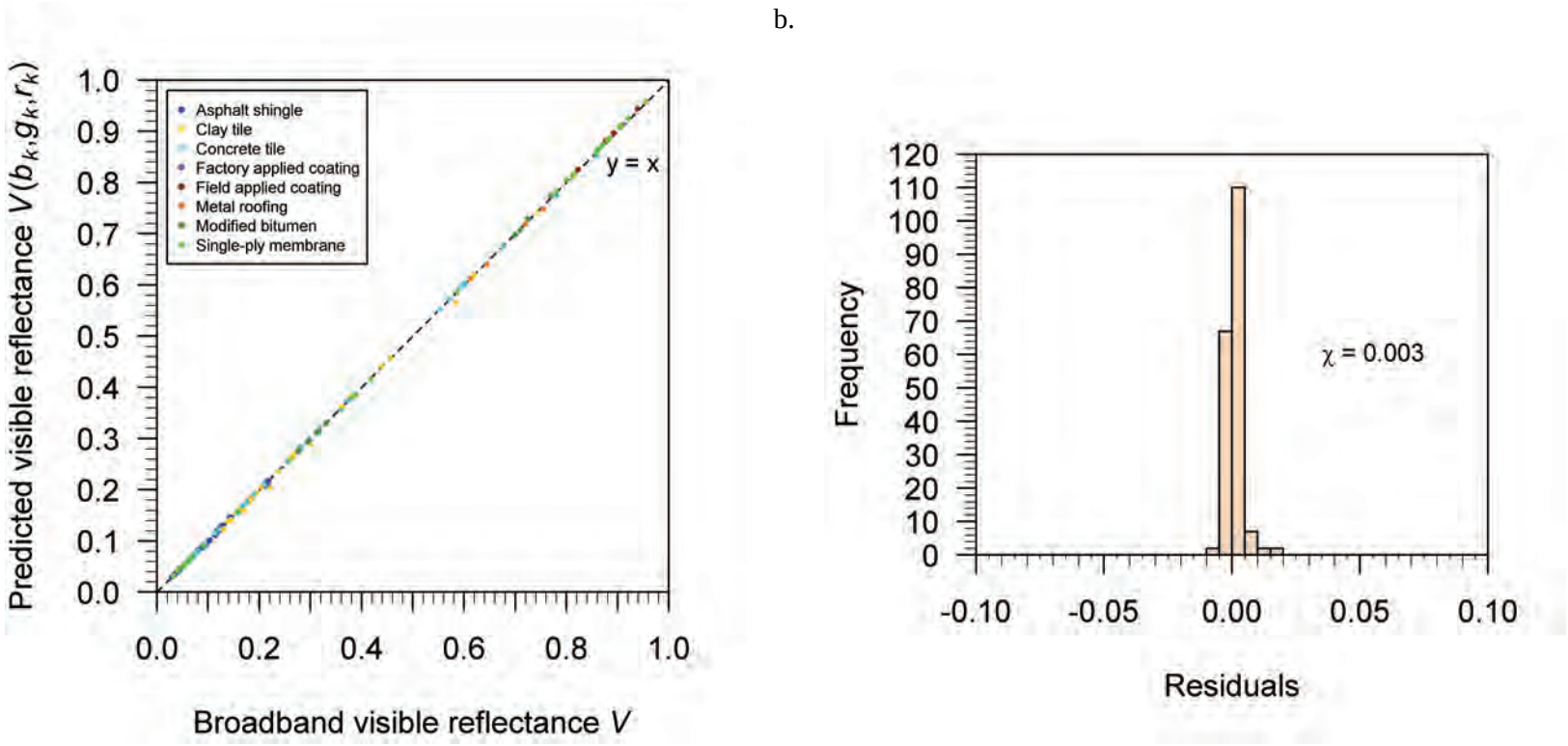

Figure 3-5. Assessment of the empirical model for relating broadband reflectances to narrowband reflectances. All values are computed using solar spectral reflectance measurements of the 190 roof samples (Table 3-2). In (a) visible reflectance $V(b_k, g_k, r_k)$ computed using Eq. (7) is compared to V_k calculated from Eq. (1). The corresponding histogram of residuals is shown in (b). χ is the root mean square of the residuals. In (c), solar reflectance (albedo) $S(b_k, g_k, r_k, i_k)$ computed using Eq. (8) is compared to S_k calculated from Eq. (1); the corresponding histogram of residuals is shown in (d).

c.

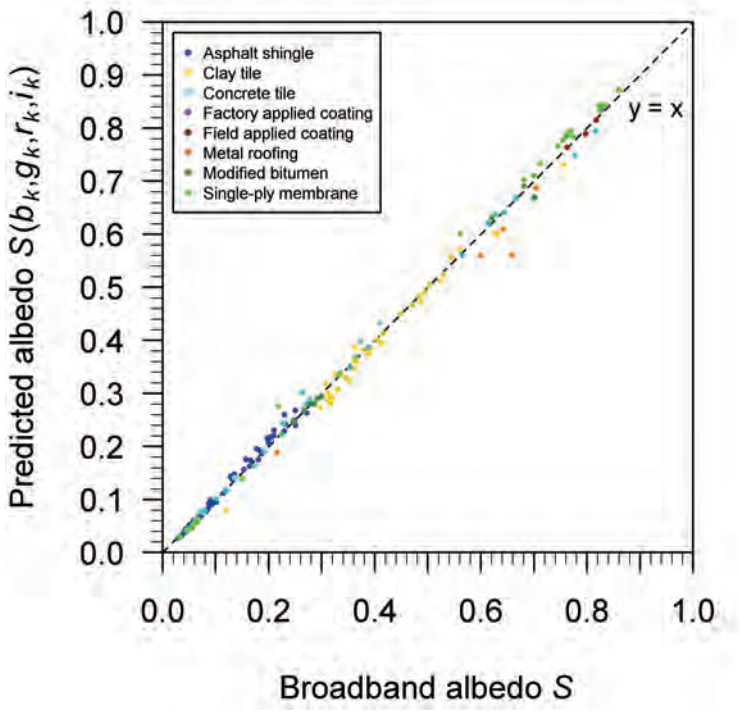

d.

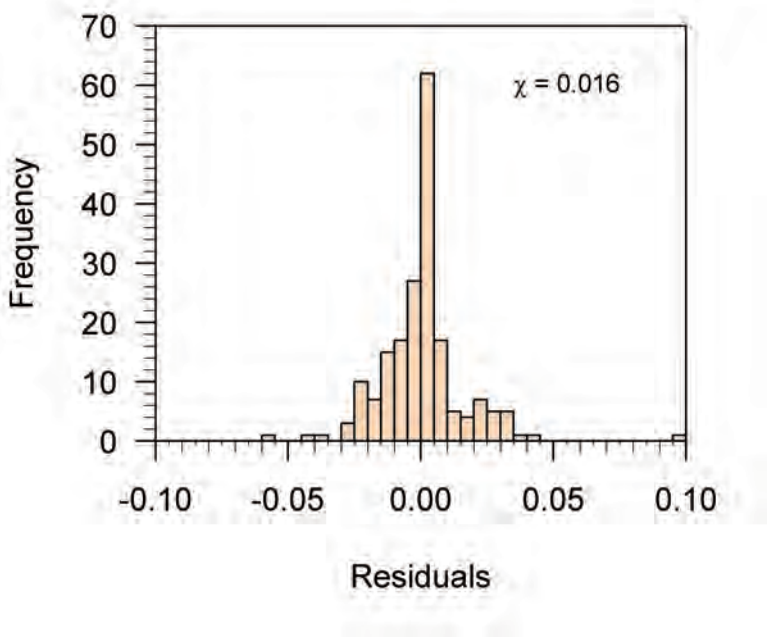

Figure 3-5 (continued)

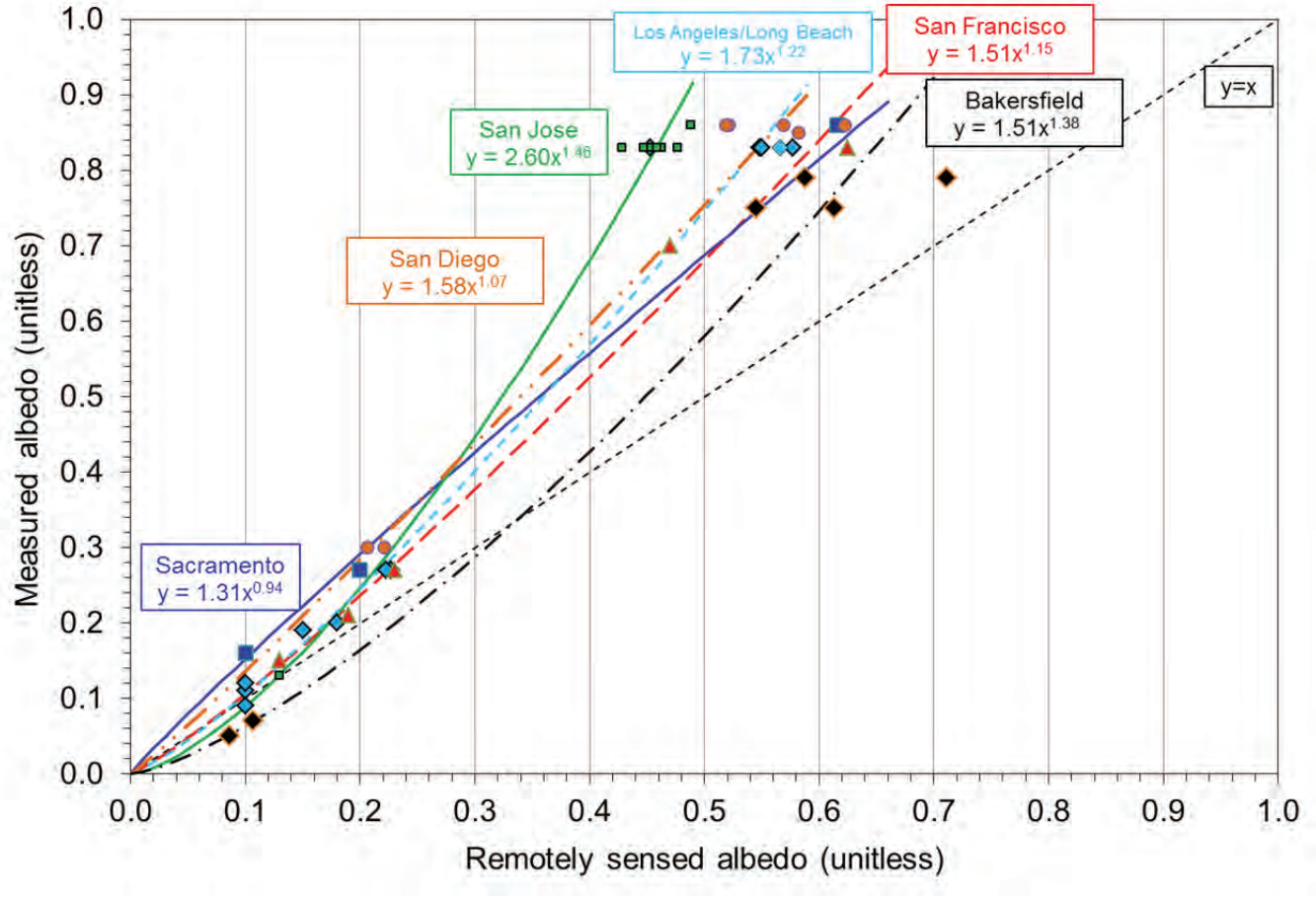

Figure 3-6. Comparison of pyranometer-measured albedos (ground truths) to (uncalibrated) remotely sensed albedos. The equations shown were applied to the uncalibrated remotely sensed albedos $S(b_k, g_k, r_k, i_k)$ to compute calibrated values S' using Eq. (3).

Figure 3-7. A portion of San Jose showing the mean (calibrated) remotely sensed albedo for each rooftop.

4. City-wide results and application to climate modeling

4.1. Overview

In Section 3 we present a new method for deriving the albedo of roofs using aerial imagery. In this section we apply the method to compute roof albedos in seven California cities: Los Angeles, Long Beach, San Diego, Bakersfield, Sacramento, San Francisco, and San Jose. First we show roof albedos projected onto maps of each city. The mean roof albedo and other statistics for each city are reported and discussed. Next, we estimate the minimum sample size required to characterize the mean albedo of the roofs in a city. This was accomplished using a Monte Carlo technique to randomly sample from the ~1.1 million roof albedos computed for Los Angeles. Next, using a large sample of duplicates we estimate the error (precision) in reported roof albedos for each city. In the Discussion section we examine the prevalence and mean albedos of roofs of different sizes; we also compute the fraction of large roofs that have high albedo. Lastly, roof albedo results for Bakersfield were used as an input to a regional climate model to estimate changes in summer and wintertime temperature and precipitation that would result from replacing the current stock of roofs with "cool" high albedo roofs.

4.2. Results

4.2.1 Roof albedos for Los Angeles, Long Beach, Bakersfield, San Francisco, and San Jose

Maps for each city showing the mean albedo of individual roofs are shown in panel a of Figure 4-1 through Figure 4-5. Panels b and c show histograms and cumulative distributions of roof albedos, respectively. In b, N is the total number of roofs, while μ and σ are the city-wide mean and standard deviation of roof albedo weighted by roof surface area; see also Table 4-1. Note that roof surface area in this report refers to the footprint area of the building. In c, we show cumulative distributions of roof albedo that are both unweighted and weighted by roof area.

Number of roofs is smallest for San Francisco (N=82,941) and largest for Los Angeles (N=1,130,120). The area fraction of each city covered by roofs ranges from 10% (Bakersfield) to 25% (San Francisco) (Table 4-1). The area-weighted mean roof albedo (± standard deviation) for each city ranges from 0.17 ± 0.08 (Los Angeles) to 0.20 ± 0.11 (Bakersfield). In each city nearly all roofs have low albedo in the range of 0.05 to 0.25 (panel b, Figure 4-1 through Figure 4-5). Roofs with albedo greater than 0.4 make up less than 3% of total roofs and 7% of total roof area in each city (panel c, Figure 4-1 through Figure 4-5); Bakersfield has the largest area fraction of roofs with albedo greater than 0.4.

Figure 4-6 presents a closer look at roof albedos in an area of Los Angeles. Some large (presumably commercial) buildings in this area have high albedo "reflective" roofs with values up to about 0.7. Many of these reflective roofs are likely the result of the Title 24 Building Energy Efficiency Standards (CEC 2005), which includes a prescription that new or retrofitted low-sloped roofs on commercial buildings should generally be white. Albedos of reflective roofs are varied because of differences in (a) initial albedo of roofs

when installed, (b) roof age, and (c) the resistance to soiling of a reflective roof, which varies by manufacturer and model (Sleiman et al. 2011).

4.2.2 Roof albedos in Sacramento and San Diego

4.2.2.1 Determining the number of roofs to manually trace

We were unable to acquire GIS building outlines from local governments for Sacramento and San Diego. We therefore manually traced buildings in ArcMap using techniques described in Section 3.1.3. The number of buildings needed to properly characterize the mean roof albedo of a city was determined using a statistical investigation of the population of ~1.1 million values computed for Los Angeles. A Monte Carlo technique was used to randomly select buildings in Los Angeles; as more randomly selected buildings were sampled, the variability in the (area-weighted) mean roof albedo decreased (Figure 4-7a). The large fluctuation at small sample sizes ($N \leq 500$ roofs) occurs because the sample mean roof albedo is very sensitive to the inclusion or absence of large high albedo roofs. As the number of samples increases, the fluctuations decrease, and an asymptote is approached representing the (area-weighted) mean roof albedo for the city. The mean roof albedo is reached after sampling about 1000 roofs (Figure 4-7a). This suggests that the mean roof albedo of Los Angeles can be characterized from the albedos of 1000 randomly sampled buildings. We expect that 1000 roofs overestimates the requirement for characterizing Sacramento and San Diego since they have fewer roofs than Los Angeles; this assertion is tested in Section 4.2.2.3.

We further investigated the effect of building sample size on city-mean roof albedo using a second set of Monte Carlo simulations. Random samples of N roofs were drawn from the total population of ~1.1 million roofs in Los Angeles. The distributions of calculated means for 100,000 such experiments are shown in Figure 4-7b for each of N = 10, 100, 1000, and 5000. Also shown are the grand means and standard deviations of sample means over the 100,000 simulated samples for each value of N. The main effect of larger sample size (N) is a narrower distribution of sample means with corresponding lower standard deviations. This shows that a randomly sampled collection of roofs is more likely to appropriately characterize the city-mean roof albedo if the sample size is larger. Our chosen sample size of 1000 roofs returns a standard deviation equal to 0.01, which is equivalent to an uncertainty with 90% confidence interval of 0.0005. This error is much smaller than the estimated error (accuracy) of the remotely sensed albedos for each roof, which is discussed in Section 3.2.2. Thus, the characterization of about 1000 randomly selected roofs in Sacramento and San Diego is unimportant as a source of uncertainty in determining their city-wide mean roof albedos.

4.2.2.2 Roof albedos

The numbers of roofs sampled in Sacramento and San Diego (about 1000 each) are orders of magnitude lower than for the other cities (Table 4-1). The area-weighted mean roof albedos for Sacramento and San Diego are 0.24 ± 0.11 and 0.29 ± 0.15 (Table 4-1, Figure 4-8 and Figure 4-9). For the buildings sampled, roofs with albedo greater than 0.4

made up about 8% and 17% of roof area in Sacramento and San Diego; these represent 5% and 2% of total roofs.

4.2.2.3 Testing the sufficiency of 1000 building outlines

Monte Carlo simulations were again performed, this time randomly sampling from the about 1000 roof albedos for Sacramento and San Diego. The sample mean roof albedos for both Sacramento and San Diego converge to the population mean at $N < 1000$ roofs (Figure 4-10). This indicates that 1000 outlines was sufficient for characterizing the (area-weighted) mean roof albedo of these two cities.

4.2.3 Precision of the remotely sensed albedos

Buildings with duplicate remotely sensed albedos were used to estimate the precision error of the albedo values. For the cities with existing outlines for all buildings, numbers of roofs with duplicate albedo values ranged from 37,344 (Long Beach) to 430,332 (Los Angeles) (Table 4-2). Sacramento and San Diego, the cities with manually traced outlines, have 80 and 548 duplicates, respectively. Figure 4-11 shows histograms of scaled arithmetic difference (see Eq. (6) in Section 3.1.7) for each city. Nearly all scaled arithmetic differences are small, indicating that the remotely sensed albedos are precise. The root-mean-square (RMS) of the scaled arithmetic differences range among the cities from 0.009 (San Diego and Sacramento) to 0.04 (San Francisco) (Figure 4-11).

4.3. Discussion

4.3.1 Disaggregating roof albedos by roof area

The stock of roofs in each city is further examined by disaggregating buildings by their footprint area. The fractions of urban roof area comprised by roofs smaller and larger than a range of thresholds was computed (Figure 4-12a,b). Corresponding area-weighted mean roof albedos both below and above a range of roof area thresholds are in Figure 4-12c,d. Note that we do not present disaggregated results for Sacramento and San Diego since in these cities we computed roof albedos for a limited number of roofs.

Most roofs in the five California cities discussed here are small. In four of the five cities shown (Los Angeles, Long Beach, Bakersfield and San Jose), small roofs (< 400 m^2) make up about 60-70% of urban roof area while large roofs[3] (> 1000 m^2) make up about 15-25% (Figure 4-12a,b). Further, half the urban roof areas are comprised of roofs that are smaller than about 300 m^2. The stock of roofs in San Francisco is somewhat different than the four other cities in that more of its roofs are large (Figure 4-12a,b).

The area-weighted mean roof albedo for small roofs (< 400 m^2) ranges among the cities from 0.14 to 0.17 (Figure 4-12c). The mean albedo for large roofs (> 1000 m^2) is more variable among the cities, ranging from 0.18 to 0.34 (Figure 4-12d). The mean albedo for

[3] These small and large roof sizes were chosen somewhat arbitrarily but are intended to roughly approximate the maximum and minimum size of homes and commercial buildings, respectively. Buildings with roof areas between 400 and 1000 m^2 are more difficult to generalize.

roofs smaller than a given area threshold is weakly sensitive to that threshold (Figure 4-12c) because of the dominance of small roofs. While large roofs have a relatively high mean albedo compared to small roofs in cities other than San Francisco (Figure 4-12d), they comprise a relatively small fraction of total city roof area (Figure 4-12b). This shows that while using reflective roofs on large buildings can increase the total roof albedo of a city, small roofs that are presumably mostly residential make up a larger fraction of urban area and urban roof area (Table 4-1). Moreover, these small roofs currently have low albedo. Therefore, increasing the albedo of roofs on residential homes could be an effective way of increasing the albedo of cities in the future. A method for estimating the urban albedo increase attainable using cool roofs is detailed in Appendix A.

4.3.2 Computing the fraction of large roofs that have high albedo

In October 2005 the California Energy Commission added to the prescriptive approach (see Appendix B) of its Title 24 Building Energy Efficiency Standards (CEC 2005) that new or retrofitted low-slope roofs on commercial buildings should generally have high albedo (CEC 2005). It is therefore of interest to calculate the fraction of low-slope roofs that had high albedo when the imagery was acquired in summer 2009. Since computing the slope of individual roofs in each city was outside the scope of this study, we used roofs with area > 5000 m^2 as a proxy for commercial buildings with low slope roofs. While many commercial buildings have footprint areas smaller than 5000 m^2, we pick this large area to ensure that the population is nearly entirely commercial buildings with low-slope roofs. In 2009, a minimum "aged" roof albedo of 0.55 was required to meet Title 24 prescriptive requirements for a reflective roof. (This minimum albedo requirement has since been increased (CEC 2008, CEC 2013).) Since some roofs contain low albedo equipment, we identified high albedo roofs in the current investigation as those with mean albedo > 0.4. Note that we do not show results for Sacramento and San Diego due to their low building sample size.

In the five cities with city-wide building outlines (Los Angeles, Long Beach, Bakersfield, San Jose, and San Francisco), roofs with area > 5000 m^2 represent $\leq$ 0.5% and $\leq$ 10% of total roofs and roof surface area, respectively (Table 4-2). Of this subset of buildings, 3% (San Francisco) to 41% (Bakersfield) of total roofs had albedo > 0.4 (Table 4-2). We note that roofs with mean albedo > 0.4 could fail to identify a high albedo roof under the following circumstances: (a) the roof supports extensive dark equipment (e.g. HVAC, photovoltaics), reducing the mean albedo to < 0.4; (b) the roof experienced extreme soiling, which could occur when improperly installed and/or near sources of pollution. Thus, we suggest that the values presented here are likely to underestimate the fraction of low-slope commercial roofs that meet the Title 24 prescriptive requirements for roof albedo. We recommend a future study that repeats our analysis to track the adoption of white roofs onto buildings in California.

4.4. Application: Predicting regional temperature changes from cool roofs

The potential for cool roofs to reduce urban temperatures in Bakersfield, California was investigated using a state-of-the-science meteorological model. The model was configured to represent the region around Bakersfield at high spatial resolution. Base case

and cool roof scenarios (referred to herein as ‘base_case’ and ‘cool_roof’) were simulated with the only difference being that the surface albedo in Bakersfield was increased under the cool roof scenario. Roof albedos presented in this study were used to derive ‘base_case’ albedos in Bakersfield. Methods for calculating albedos in the ‘cool_roof’ scenario are described below. Summer and winter afternoon temperature changes that result from increasing roof albedo were quantified by subtracting ’base_case’ scenario results from those of the ‘cool_roof’ scenario (i.e. ‘cool_roof’ minus ‘base_case’). Changes in summer and winter accumulated precipitation were similarly calculated.

4.4.1 Modeling setup

The Weather Research and Forecasting model, WRF version 3.4.1 (Skamarock et al. 2008) was configured with a “two-way” nested domain; an inner domain of 97.5 × 97.5 km with 1.3 × 1.3 km resolution was centered in Bakersfield, and a 36 × 36 km resolution outer nest covered the remainder of California. Boundary and initial conditions were from the NCEP North American Regional Reanalysis (NARR) (Mesinger et al 2006). Longwave and shortwave radiative transfer through the atmosphere was modeled within WRF using the Rapid Radiative Transfer Model (RRTMG). Atmospheric physics in the model surface layer was based on Eta similarity, which uses Monin-Obukhov with Zilitinkevich thermal roughness length and standard similarity functions from look-up tables (Skamarock et al. 2008). The planetary boundary layer physics used the Mellor-Yamada-Janjic scheme. Cumulus clouds in the coarse outer domain were parameterized using the Grell 3d ensemble cumulus scheme; these clouds were resolved in the higher resolution inner domain and thus no parameterization was needed. The Noah Land Surface Model was coupled to the atmosphere model. This land model uses surface albedo inputs (among other land properties) to compute the surface energy balance.

Albedos in non-urban grid cells and urban cells outside of Bakersfield were computed using monthly mean values from the MODerate resolution Imaging Spectroradiometer (MODIS) as distributed with WRF version 3.4.1. Albedos within Bakersfield for the ‘base_case’ and ‘cool_roof’ scenarios were computed as described in the next section.

Each scenario was simulated as a series of 20 weeklong episodes representing the first weeks of February, June, August, and December for the years 2005 – 2009. Winter afternoon temperature changes from increasing roof albedo were computed as the mean change at 15:00 LST in December and February, while summer afternoon temperature changes were computed from the June and August results. Winter and summer changes in precipitation were calculated similarly but used weekly totals to calculate seasonal values.

4.4.2 Computing albedos for the ‘base_case’ and ‘cool_roof’ scenarios

Grid-cell mean surface albedo inputs for climate models are often derived from satellite observations. For example, WRF provides two default satellite-derived albedo inputs, one of which uses monthly mean MODIS observations from 2001. The corresponding annual mean of the monthly albedos is shown in Figure 4-13a.

In this work, we use remotely sensed roof albedo results presented in this report to estimate grid cell level albedos in Bakersfield as follows. First, buildings were classified as having low-slope versus pitched roofs. As discussed in Section 4.3.1, buildings with low-slope roofs were assumed to be those with footprint area ≥ 1000 m^2. The remainder of buildings were assumed to have pitched roofs. Next, area-weighted mean roof albedos corresponding to WRF model grid cells were computed for these two building categories. Then, grid cell mean albedos were calculated as

$$S_{\text{grid\_cell}} = S_{\text{roof pitched}} \times f_{\text{roof pitched}} + S_{\text{roof low-slope}} \times f_{\text{roof low-slope}} + S_{\text{pavement}} \times f_{\text{pavement}} + S_{\text{other}} \times f_{\text{other}} \quad (9)$$

where S is albedo and f is fraction of the grid cell covered by the corresponding land cover type described in the subscript. Subscripts 'roof_pitched' and 'roof_low-slope' correspond to pitched and low-slope roofs, respectively. Values of S and f for the 'base_case' scenario were derived using the roof albedo results developed in this report. In the 'cool_roof' scenario $f_{\text{roof pitched}}$ and $f_{\text{roof low-slope}}$ were the same as in 'base_case', while values of $S_{\text{roof pitched}}$ and $S_{\text{roof pitched}}$ were 0.35 and 0.60, corresponding to "aged" albedos of currently available cool dark and white roofing materials, respectively (CRRC, 2013).

Subscript 'pavement' corresponds to pavement surfaces with S_{pavement} assumed[4] to be 0.14 and f_{pavement} computed as

$$f_{\text{pavement}} = (f_{\text{roof pitched}} + f_{\text{roof low-slope}}) \times P \quad (10)$$

where P = 1.4 is the average ratio of pavement to roof area in a typical urban environment (Akbari et al. 2009).

Subscript 'other' corresponds to land cover types other than roofs and pavements where

$$f_{\text{other}} = 1 - (f_{\text{roof pitched}} + f_{\text{roof low-slope}} + f_{\text{pavement}}) \quad (11)$$

S_{other} is estimated as the corresponding albedo value derived from the monthly mean MODIS observations distributed with WRF. Values of f_{other} are low in Bakersfield. Thus, the product $f_{\text{other}} \times S_{\text{other}}$ is low and $S_{\text{grid\_cell}}$ (Eq. (9)) within the city is determined mostly from roof and pavement albedos. Note that albedos outside of Bakersfield are determined using only MODIS observations.

[4] Past studies (Pomerantz et al. 1997, 2000a,b; Pomerantz and Akbari 1998) indicate that the albedo of aged asphalt pavement can range from 0.10 – 0.18. We assume a pavement albedo of 0.14, which is in the middle of this range.

Annual mean albedos ($S_{\text{grid\_cell}}$) used in the 'base_case' scenario are shown in Figure 4-13b. Values are nearly the same as default MODIS-derived albedos (Figure 4-13a), though several grid cells have slightly higher albedos, presumably partly due to white roofs installed between 2001 (MODIS observations) and 2009 (aerial imagery). Annual mean albedos used in the 'cool_roof' scenario (Figure 4-13c) are up to 0.05 higher than in the 'base_case' scenario.

4.4.3 Comparing 'base_case' scenario simulations to observations

"Base_case' scenario surface air temperatures (summer and winter) were compared to observations obtained from the Global Surface Summary of the Day product available from the National Climatic Data Center, station 723840-23155 (Meadows Field Airport in Bakersfield). Modeled temperatures were computed using the grid cell containing the point-measurement location of the observations.

Linearly regressing modeled to observed temperatures resulted in coefficients of determination of 0.92 and 0.91 for mean and maximum daily temperatures, respectively. The mean biases (model – observation) in daily mean and maximum temperatures were 0.8 K and 0.3K, respectively.

4.4.4 Simulated changes in surface air temperature from cool roofs

Average temperature differences between the 'base_case' and 'cool_roof' scenarios were calculated each week and variation across the simulations was used to calculate statistical significance at the 95% confidence level. Seasonal average afternoon (15:00 LST) temperature changes are presented in Figure 4-14. Afternoon temperatures are reduced by up to 0.2 °C across Bakersfield during both the summer and winter. While temperature changes are similar during winter and summer, only summer shows statistically significant temperature changes downwind (southeast) of Bakersfield. This indicates that reduced summertime temperatures may be felt over a distance that is 2 or 3 times the length scale of the region with cool roofs.

Model estimates of temperature changes from increasing urban albedo are sensitive to (a) the magnitude of the assumed albedo increase, (b) the way in which urban areas are represented in the model, (c) local meteorology of the city being investigated, and (d) the time period of the model simulations and analysis. Temperature changes modeled in this study are smaller than changes predicted by another study (Taha 2008b) that simulated the effects of reflective surfaces for Sacramento, California. While Taha modeled daytime temperature reductions of up to 3° C, the assumed albedo increases for urban grid cells were up to ~3x larger than in our study since he was investigating the effects of reflective roofs, pavements, and exterior walls. A second difference between Taha (2008b) and our work is that he reported temperature changes for a four-day high ozone episode, whereas temperature changes reported here are averaged over 10 model weeks per season (2 weeks per season × 5 years). By averaging over this longer time period we are representing climatic seasonal means instead of a particular meteorological regime.

A more direct comparison to our work is the predicted urban temperature reductions from reflective roofs and pavements in cities throughout the United States reported in Millstein and Menon (2011). Although Millstein and Menon (2011) used a modeling resolution (25 × 25 km) coarser than that in the current study, the summertime afternoon temperature sensitivity to albedo changes was found to be similar in California cities. For example, in response to albedo increases of 0.03, average temperature reductions in San Jose and San Diego were 0.23 °C and 0.13 °C, respectively. This is similar to simulated air temperature reductions in Bakersfield of 0.2 °C for grid cells with albedo increases of 0.05.

4.4.5 Simulated changes in precipitation from cool roofs

Changes in precipitation due to cool roofs ('cool_roof' minus 'base_case'; not shown) were found to be small and not statistically significant. Past regional climate modeling studies (Millstein and Menon 2011; Georgescu et al. 2012) have shown that in some cases reflective urban surfaces can lead to reduced precipitation. Millstein and Menon (2011) noted such decreases in summertime cumulus precipitation in the Southeastern United States. Georgescu et al. (2012) studied the climate of Phoenix, Arizona where annual precipitation is dominated by monsoon thunderstorms in the late-summer. In our study there were few instances of cumulus precipitation near Bakersfield.

Table 4-1. Number of roofs, total roof surface area, and mean and standard deviation of roof albedos for each city.

City	Total roofs analyzed	Roofs with duplicate albedos	Total roof area (km^2)	Fraction of city covered by roofs (%)	Mean albedo ± standard deviation [a]
Los Angeles	1,130,120 [b]	430,332	222.4	18	0.17 ± 0.08
Long Beach	136,582 [b]	37,344	26.9	20	0.18 ± 0.09
Bakersfield	109,237 [b]	53,541	30.5	10	0.20 ± 0.11
San Francisco	82,941 [b]	72,045	31.8	25	0.18 ± 0.08
San Jose	297,914 [b]	124,834	64.2	14	0.18 ± 0.12
Sacramento	1009 [c]	80	N/A	N/A	0.24 ± 0.11
San Diego	1003 [c]	548	N/A	N/A	0.29 ± 0.15

[a] Mean and standard deviation weighted by the footprint area of each building

[b] GIS outlines for every building in the city obtained from local city governments (see Section 3.1.3 and Table 3-1)

[c] Building outlines traced manually in ArcMap

Table 4-2. Properties for roofs with area > 5,000 m^2.

City	Percent of total roofs	Percent of total roof area	Percent with albedo > 0.4
Los Angeles	0.1	7	8
Long Beach	0.2	9	14
Bakersfield	0.1	4	40
San Francisco	0.5	10	3
San Jose	0.2	10	22

a

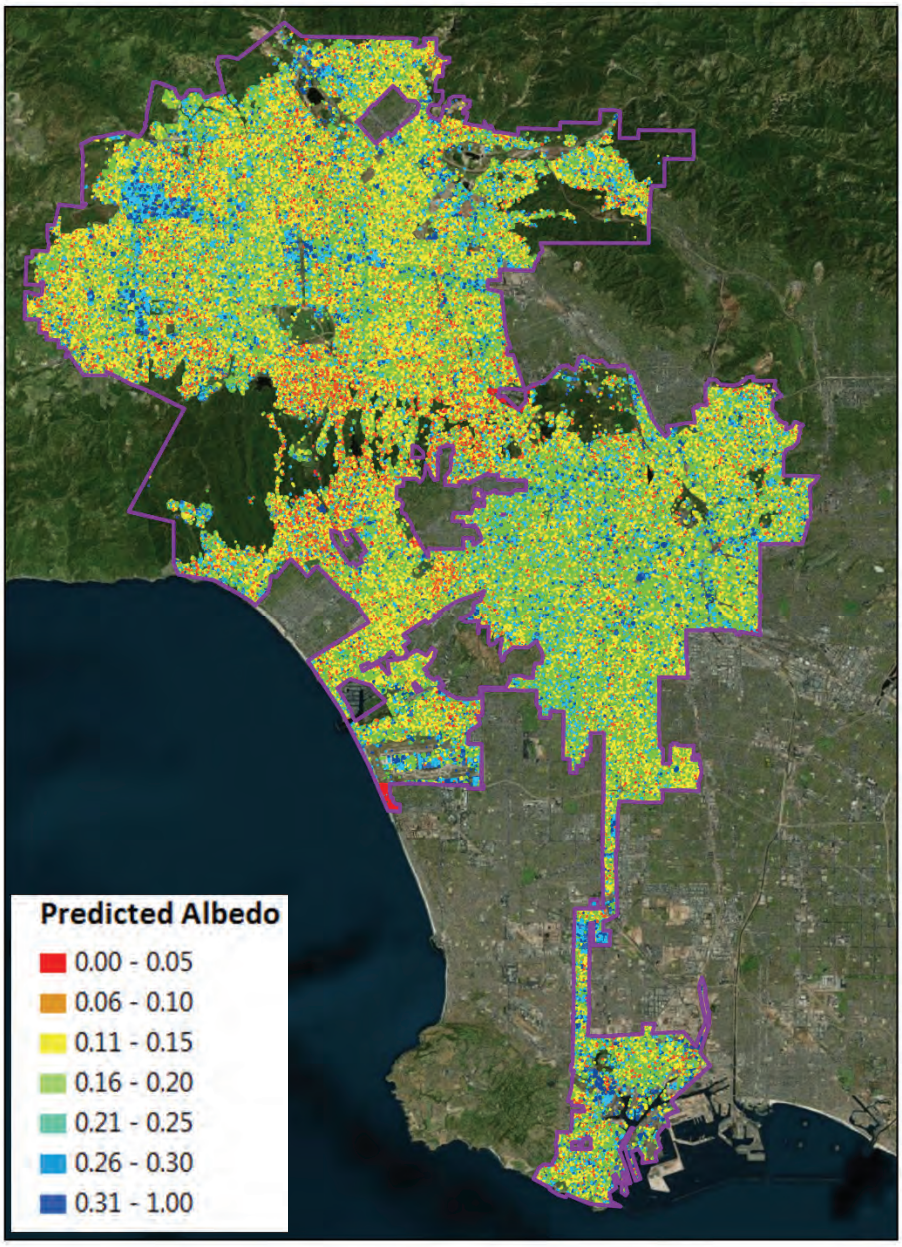

Figure 4-1. Roof albedos derived from the remotely sensed imagery for the City of Los Angeles. Roof albedos for each building within city boundaries (indicated by the magenta outline) are projected onto a map in (a). A histogram of roof albedos is shown in (b); *N* is the total number of roofs, μ is the mean roof albedo weighted by roof surface area, and σ is the standard deviation of roof albedos also weighted by surface area. Roof-area weighted (dashed) and non-weighted (solid) cumulative distribution functions (CDFs) are shown in (c). The area-weighted CDF (c) represents the cumulative fraction of roof area, whereas the unweighted curve represents cumulative fraction of roofs.

b

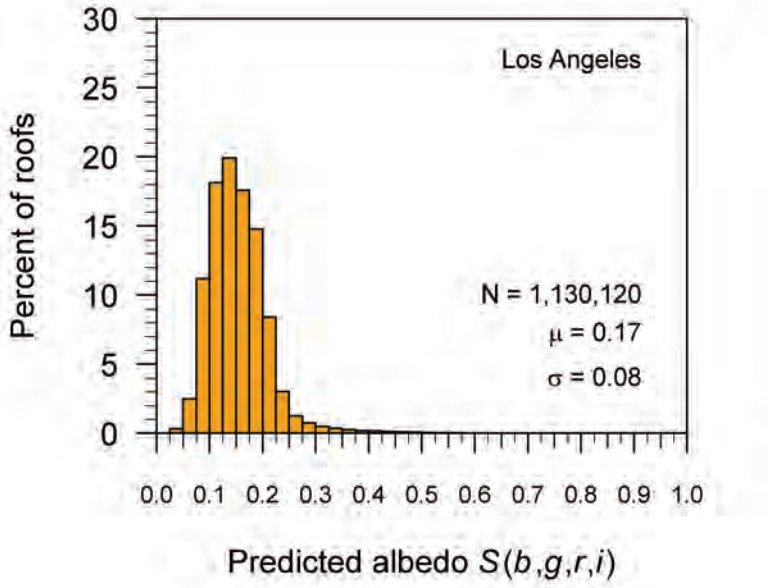

c

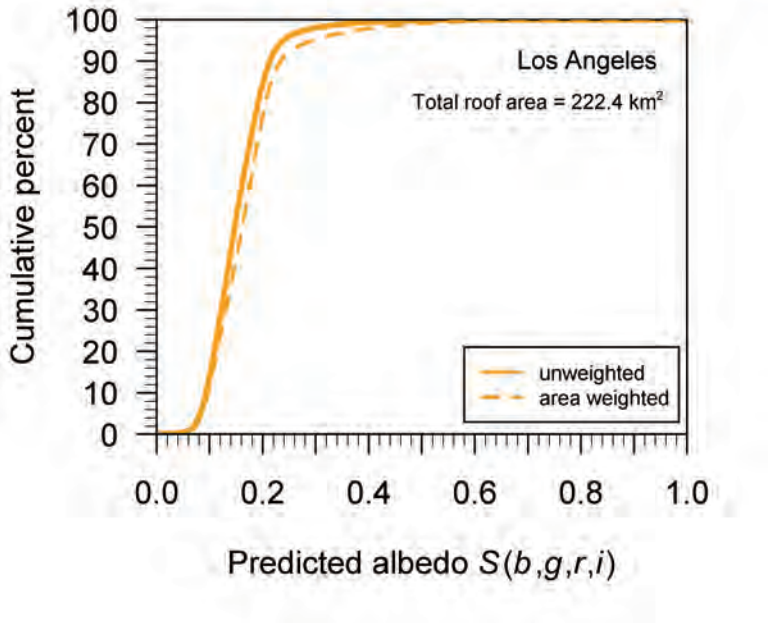

Figure 4-1 (continued)

a

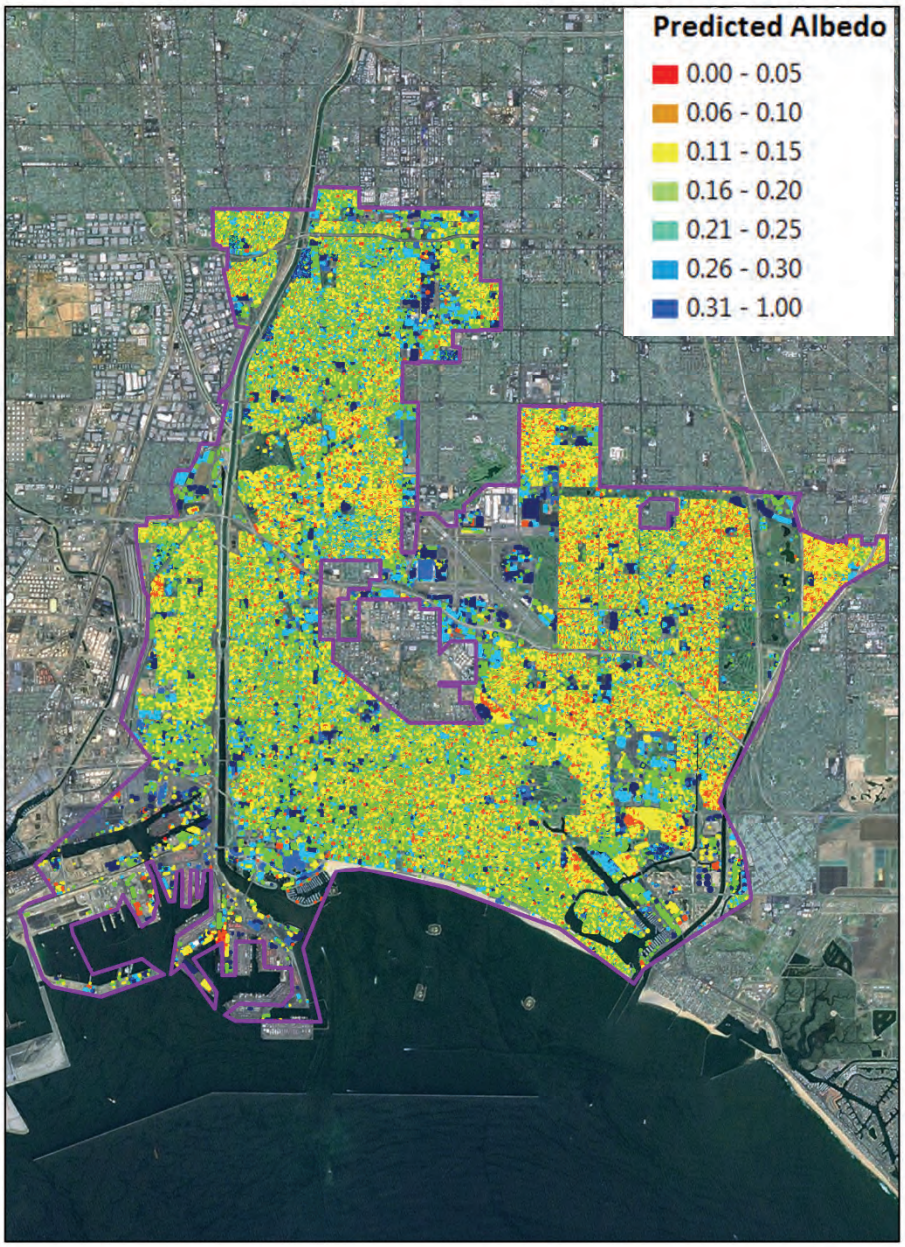

Figure 4-2. Similar to Figure 4-1 but for Long Beach.

b

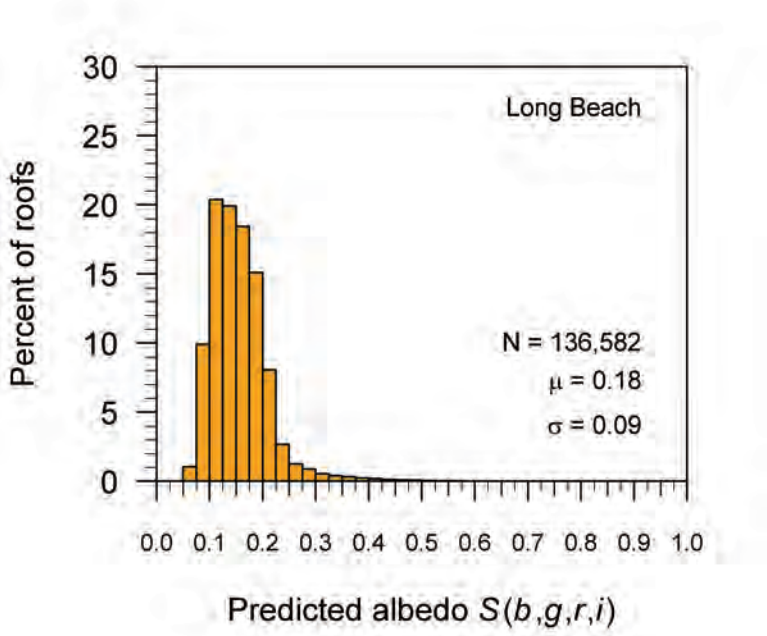

c

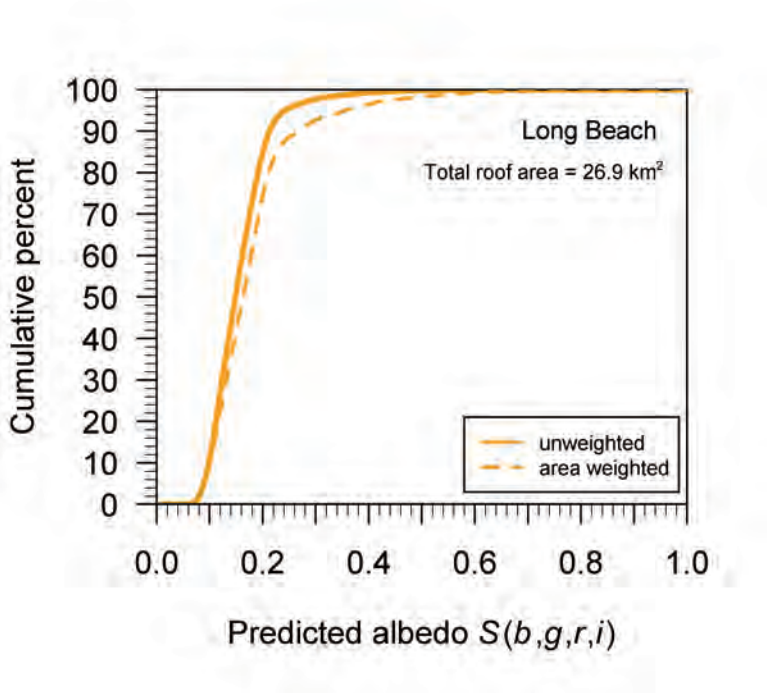

Figure 4-2 (continued)

a

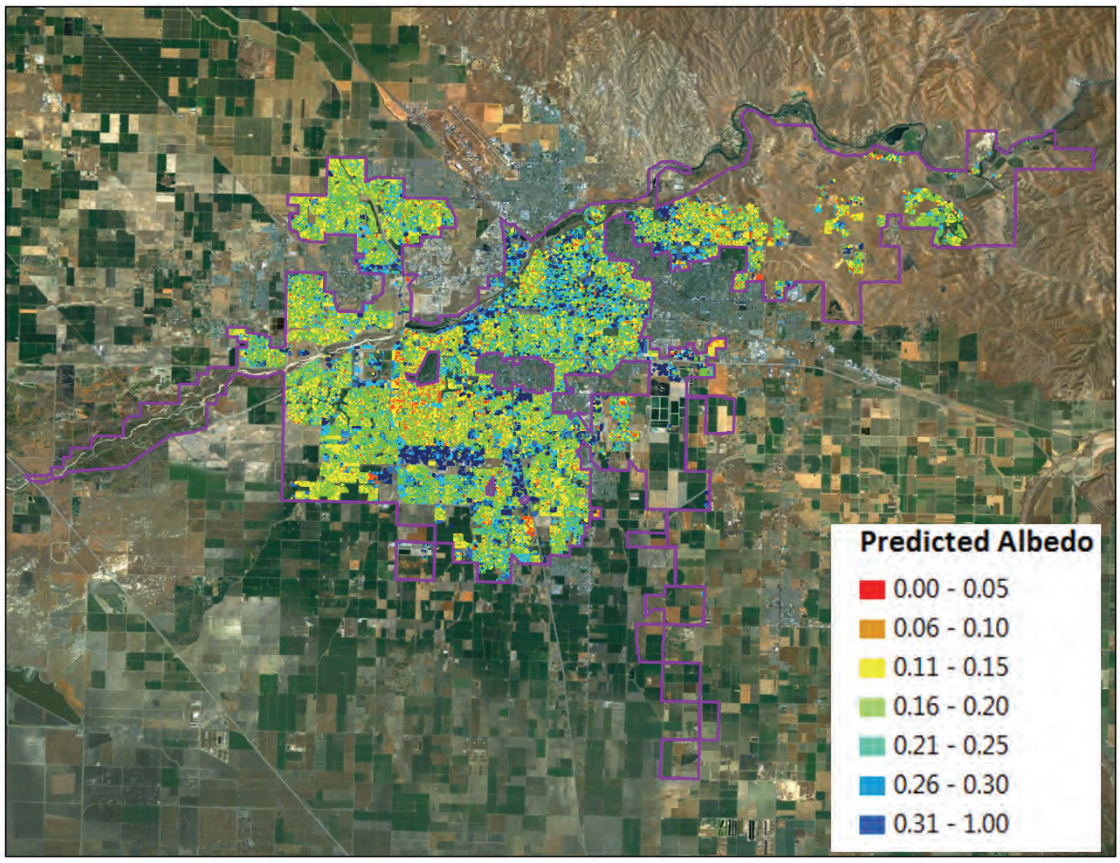

Figure 4-3. Similar to Figure 4-1 but for Bakersfield.

b

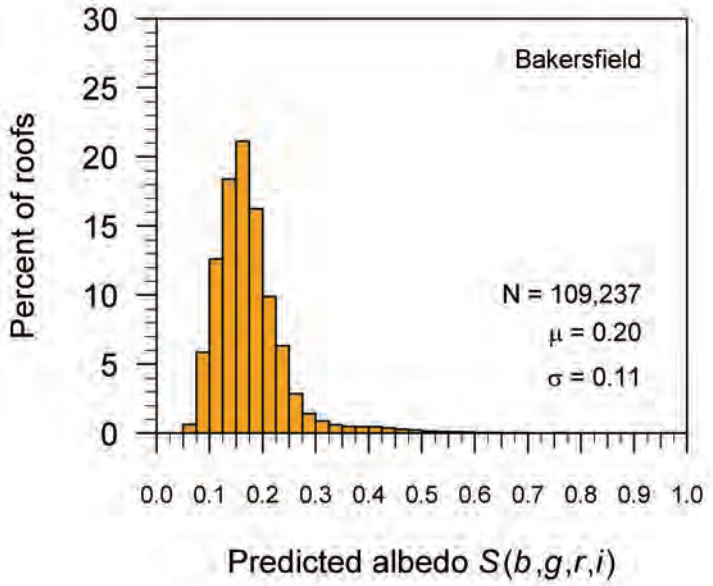

c

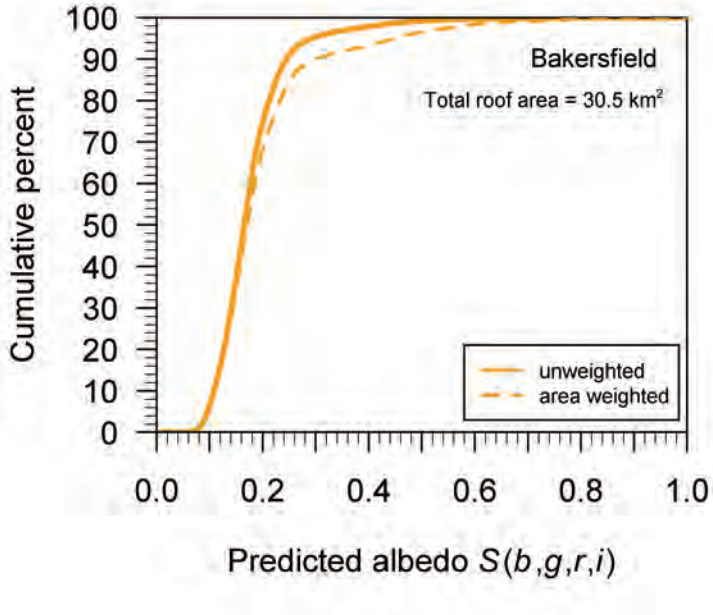

Figure 4-3 (continued)

a

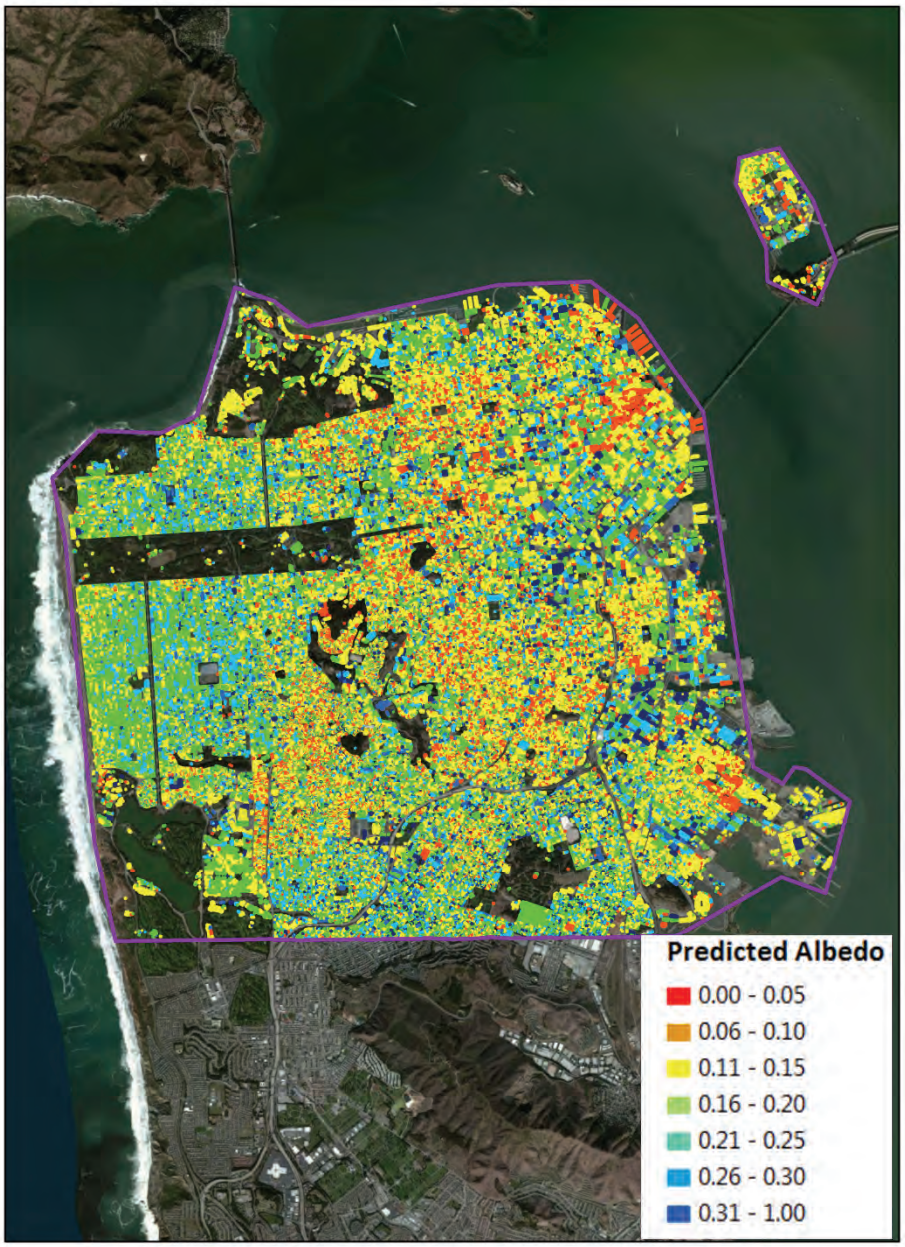

Figure 4-4. Similar to Figure 4-1 but for San Francisco.

b

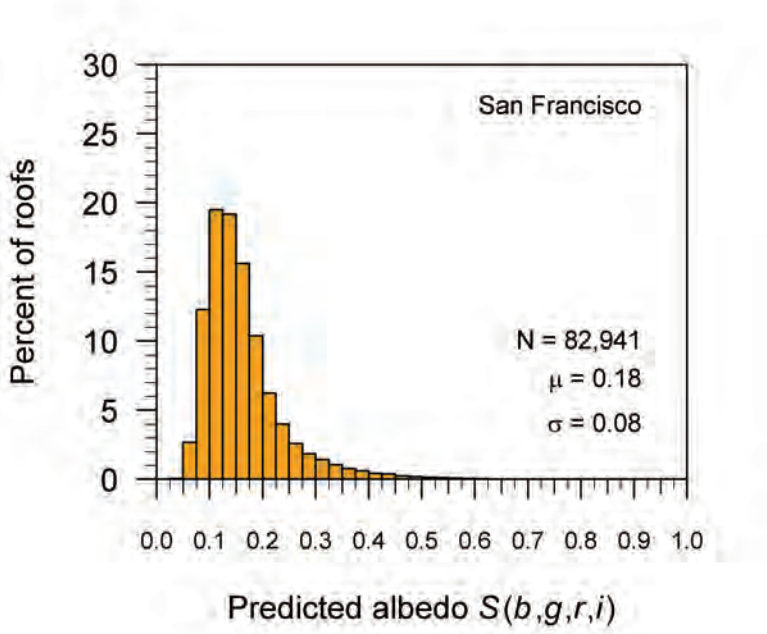

c

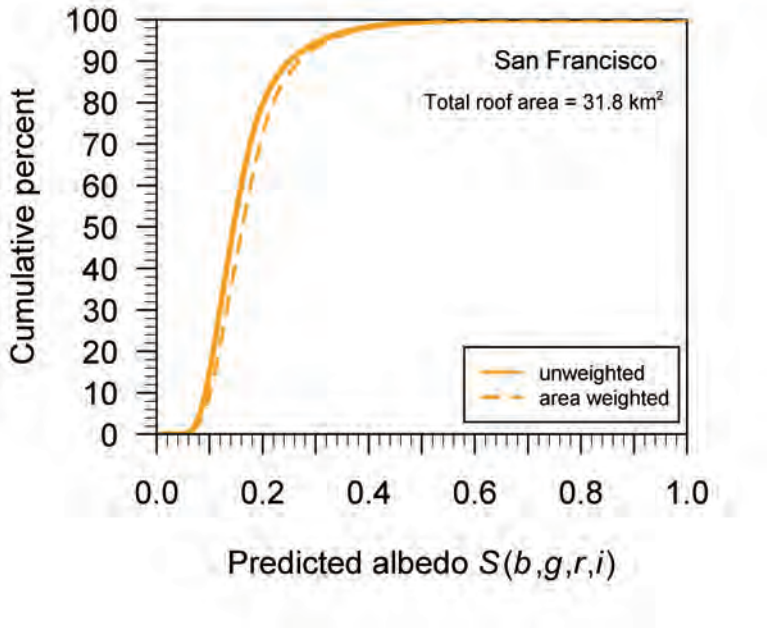

Figure 4-4 (continued)

a

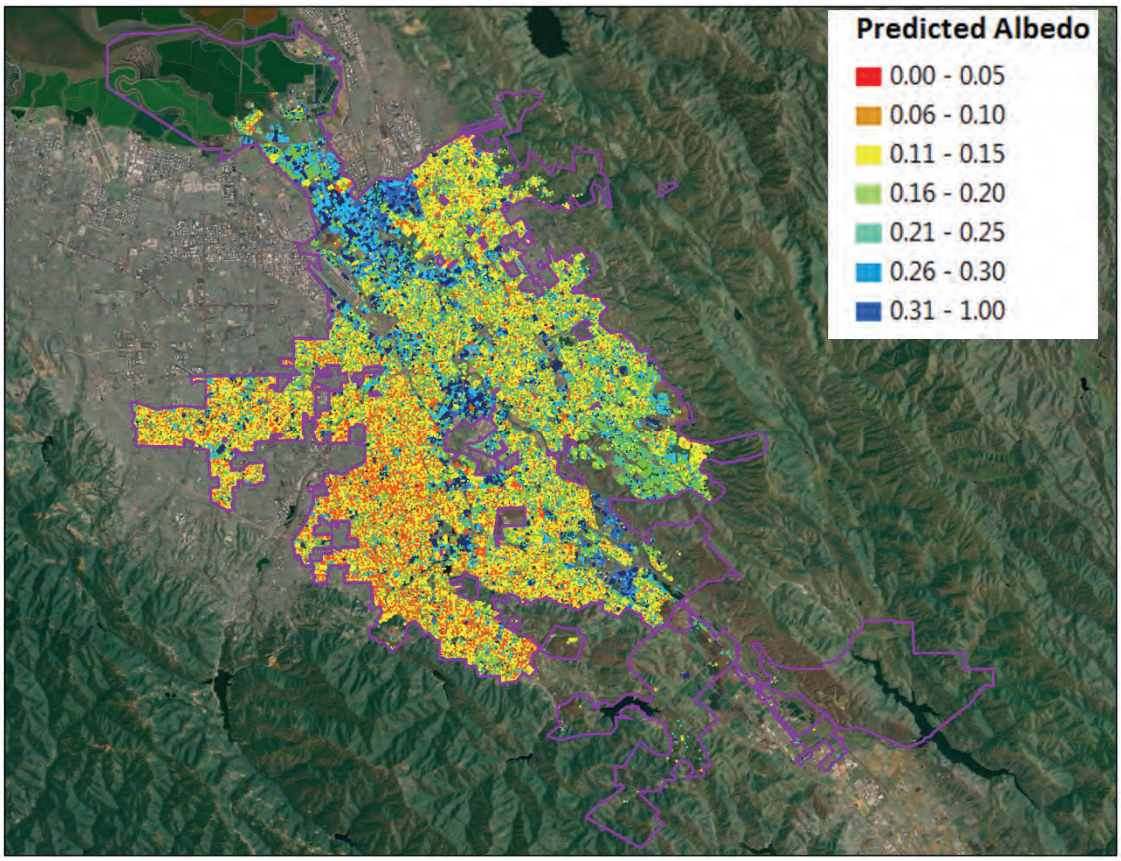

Figure 4-5. Similar to Figure 4-1 but for San Jose.

b

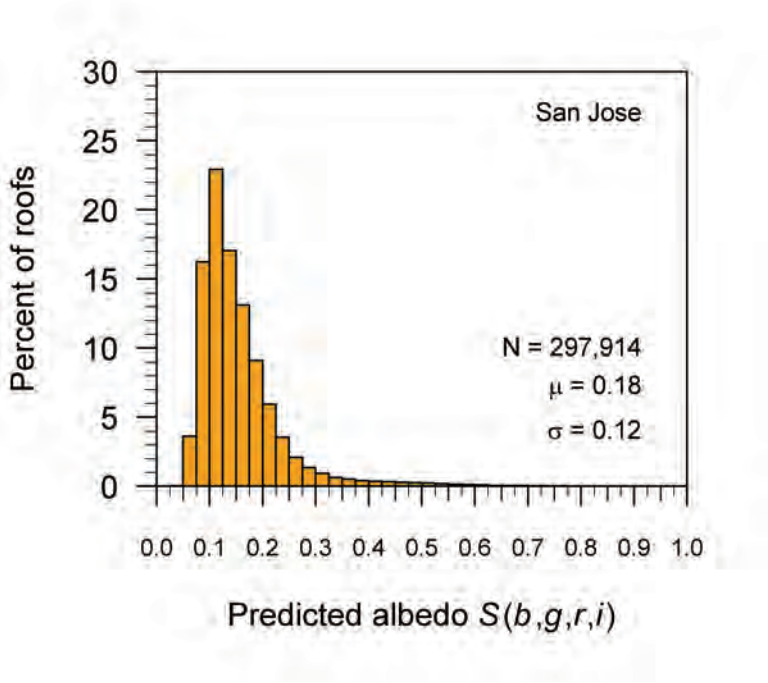

c

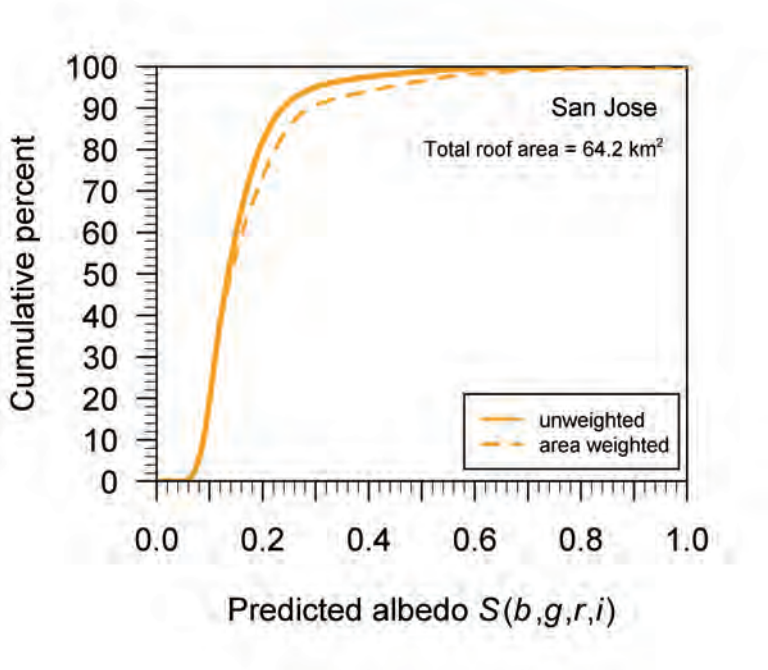

Figure 4-5 (continued)

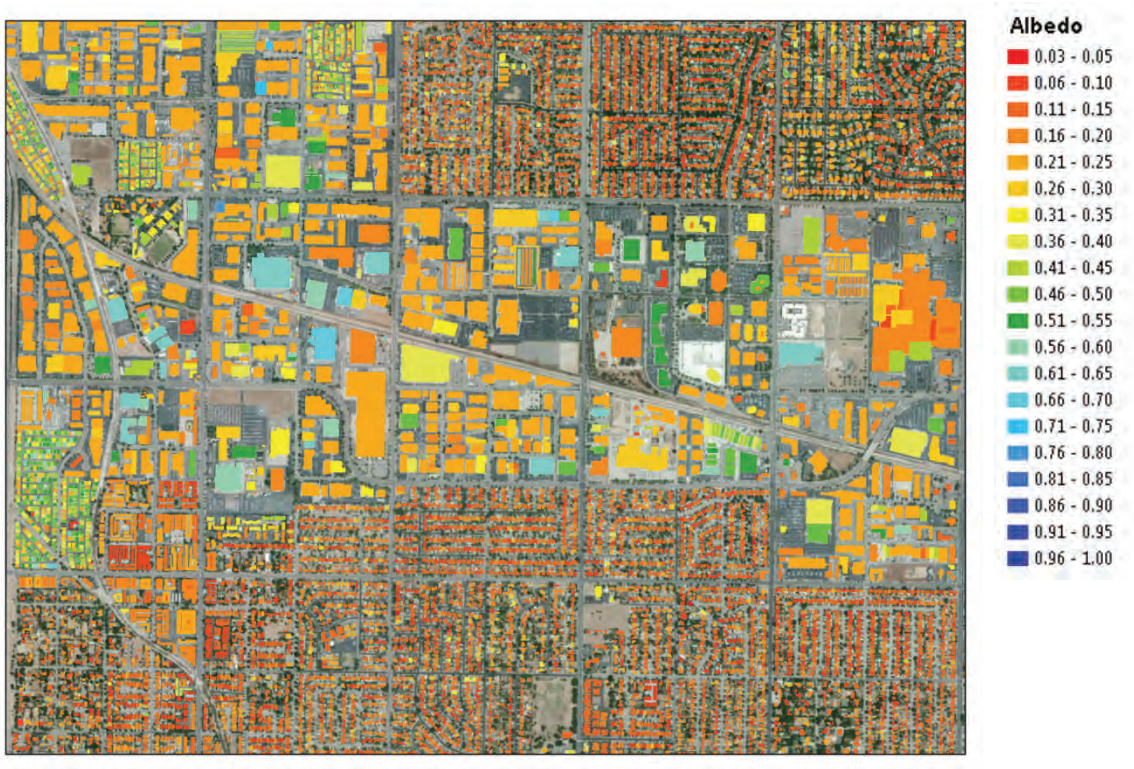

Figure 4-6. Zoomed in area of Los Angeles showing large buildings with both low and high albedo roofs. Note that the color map in this figure is different than Figure 4-1 to highlight variation in high albedo values.

a

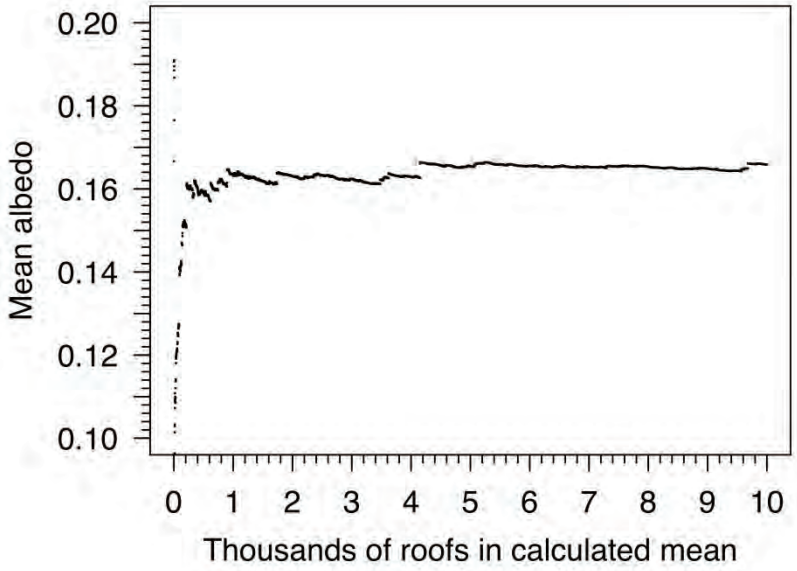

b

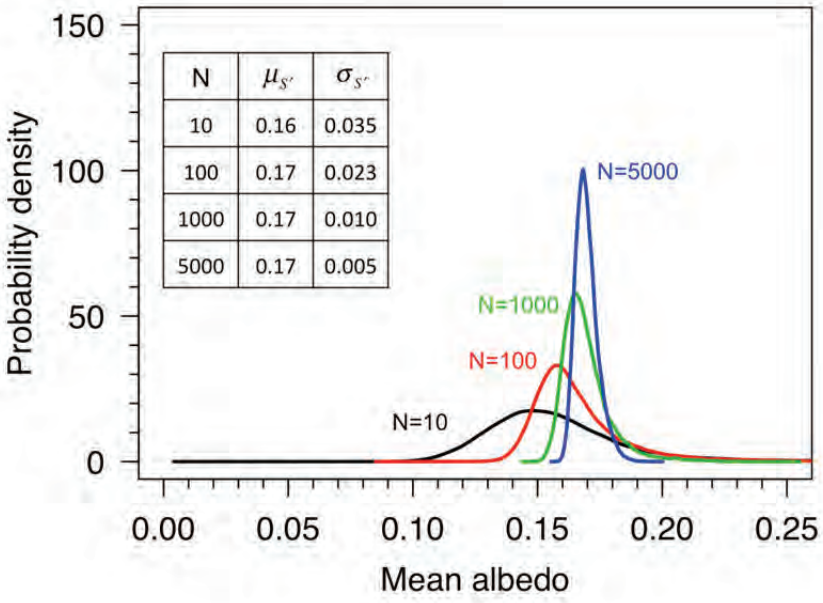

N	$\mu_{S'}$	$\sigma_{S'}$
10	0.16	0.035
100	0.17	0.023
1000	0.17	0.010
5000	0.17	0.005

Figure 4-7. Statistical investigations for determining the minimum number of building outlines needed to calculate the mean albedo of a city. Monte Carlo techniques were used to randomly select buildings from the ~1.1 million roof albedos in Los Angeles (shown in Figure 4-1). The evolution of roof area weighted mean albedo as number of roofs included in the sample mean increases is shown in (a). The probability distribution functions of simulated sample means of roof albedo for N = 10, 100, 1000, and 5000 are presented in (b). Tabulated values are number of roofs (*N*), grand mean of sample means ($\mu_{S'}$), and weighted standard deviation ($\sigma_{S'}$) of the sample means over 100,000 simulated samples (with replacement) from the population of ~1.1 million roof albedos in Los Angeles.

a

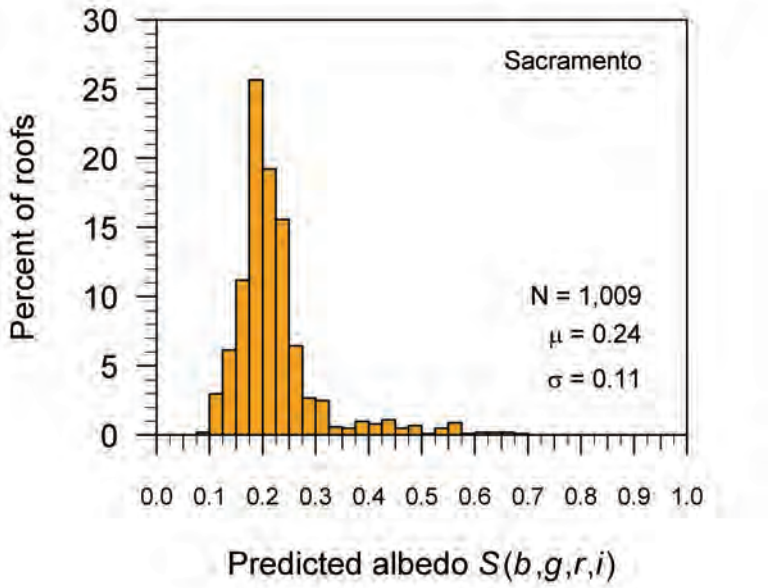

b

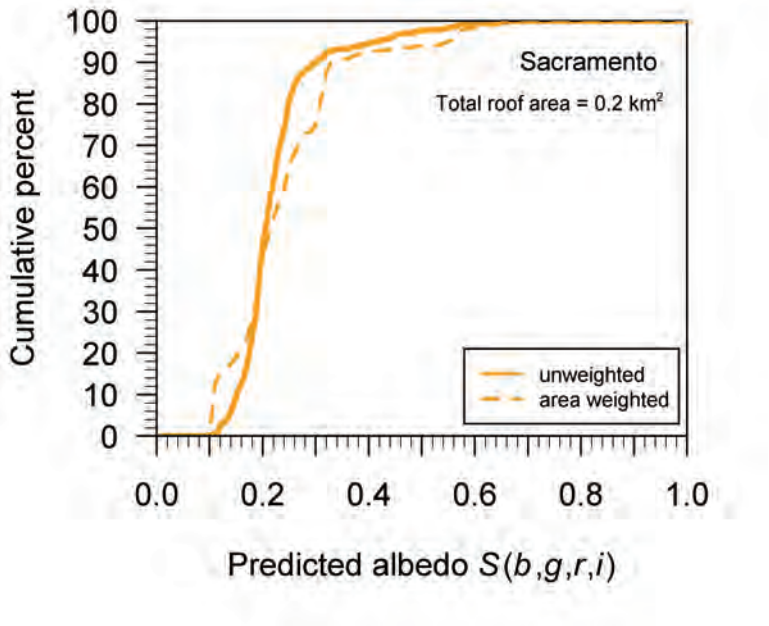

Figure 4-8. Similar to Figure 4-1 but for Sacramento. Maps are not shown due to the limited sample size.

a

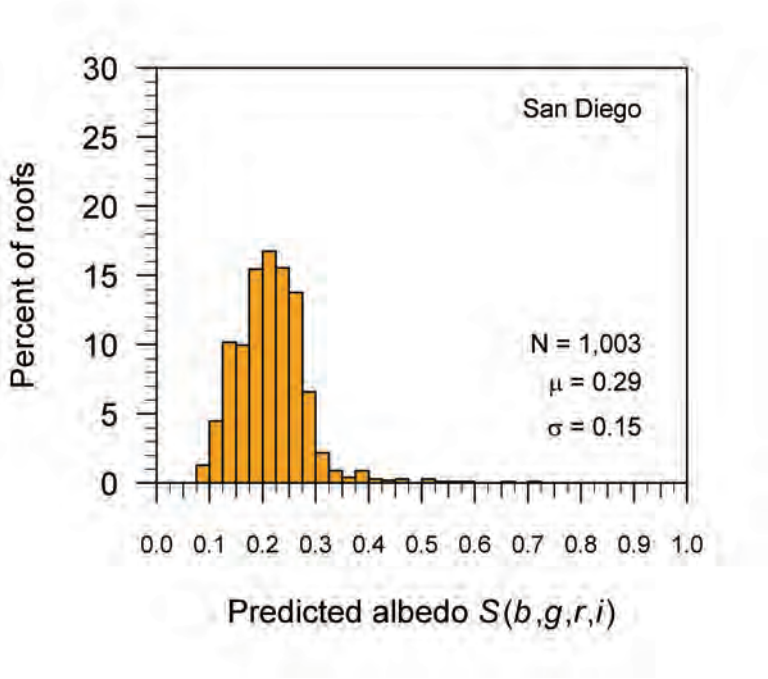

b

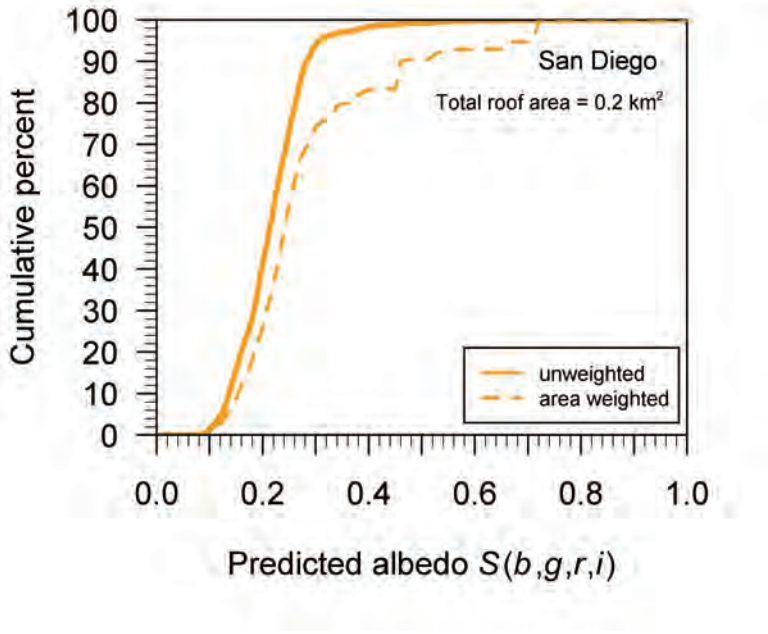

Figure 4-9. Similar to Figure 4-1 but for San Diego. Maps are not shown due to the limited sample size.

a

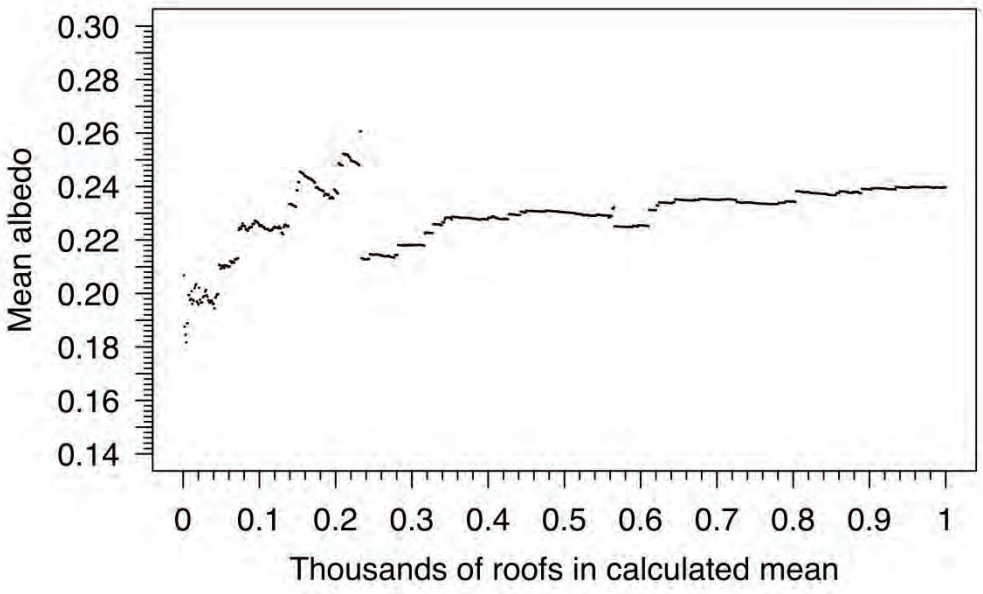

b

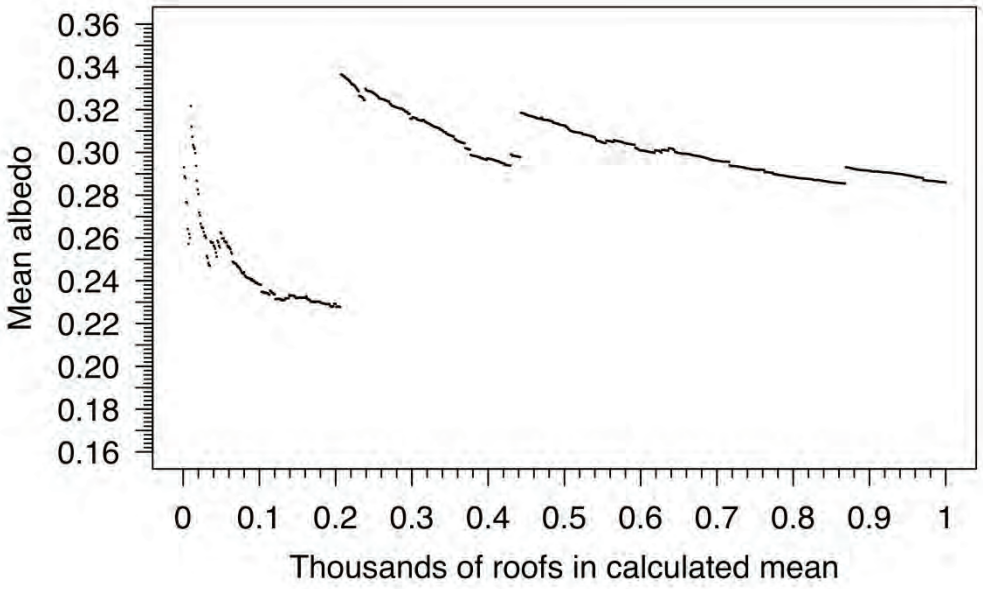

Figure 4-10. Statistical investigations to test the sufficiency of 1000 roof outlines in (a) Sacramento and (b) San Diego. See Figure 4-7a for further explanation.

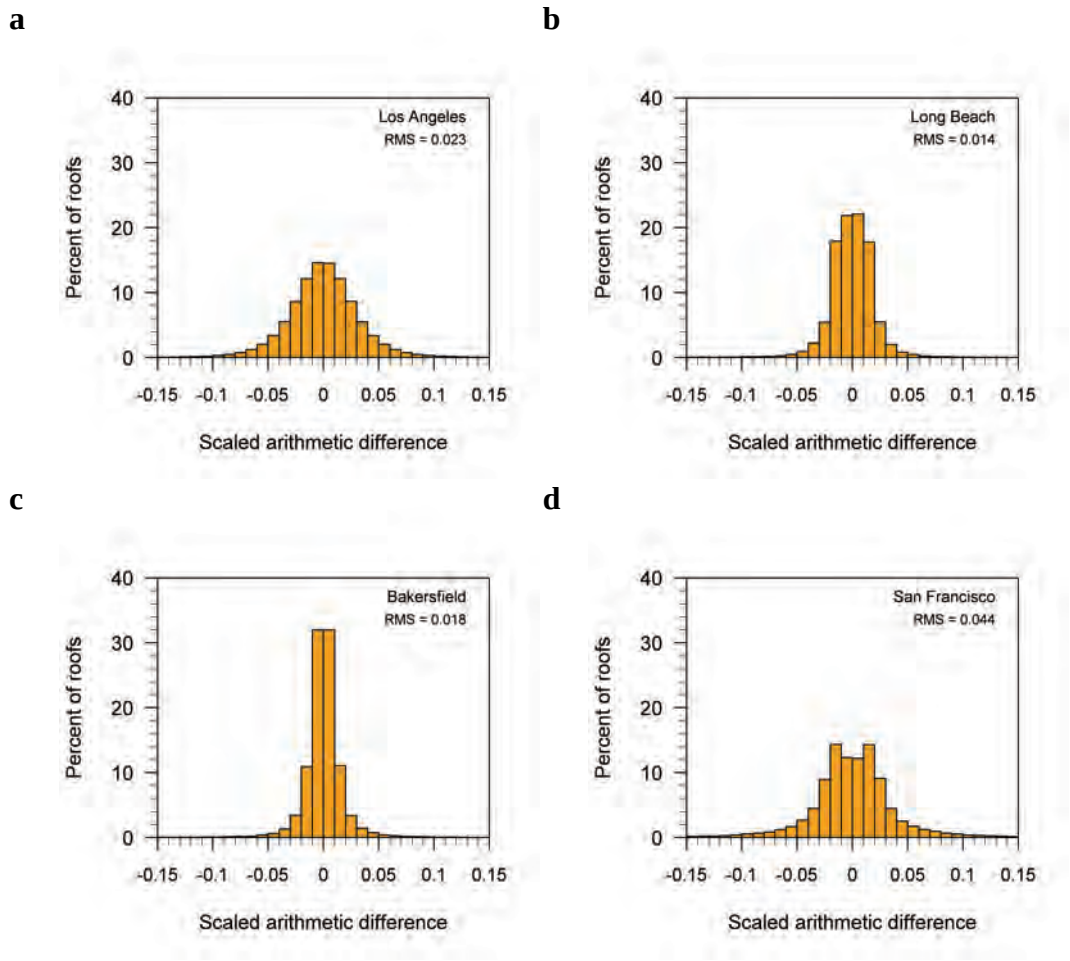

Figure 4-11. Histograms and root-mean-square (RMS) of scaled arithmetic difference for roofs with duplicate albedos. Duplicate values occurred in areas with overlap of flight paths. The number of duplicate values for each city is in Table 4-1. A small fraction of roofs had arithmetic difference greater than the horizontal axis range shown. These roofs were included in the calculation of RMS.

e

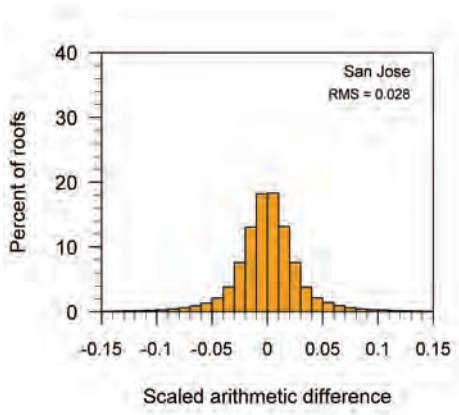

f

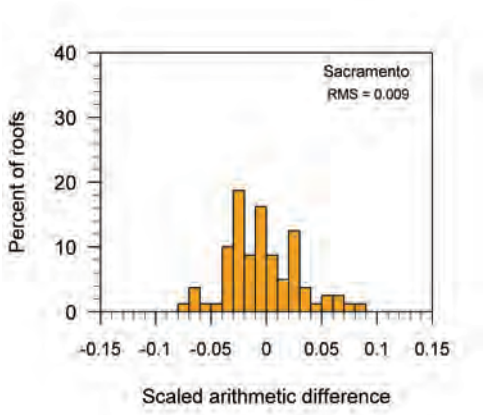

g

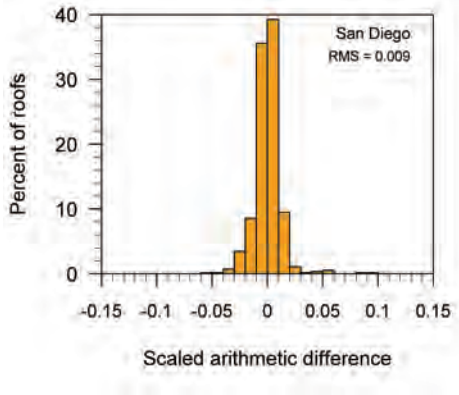

Figure 4-11 (continued)

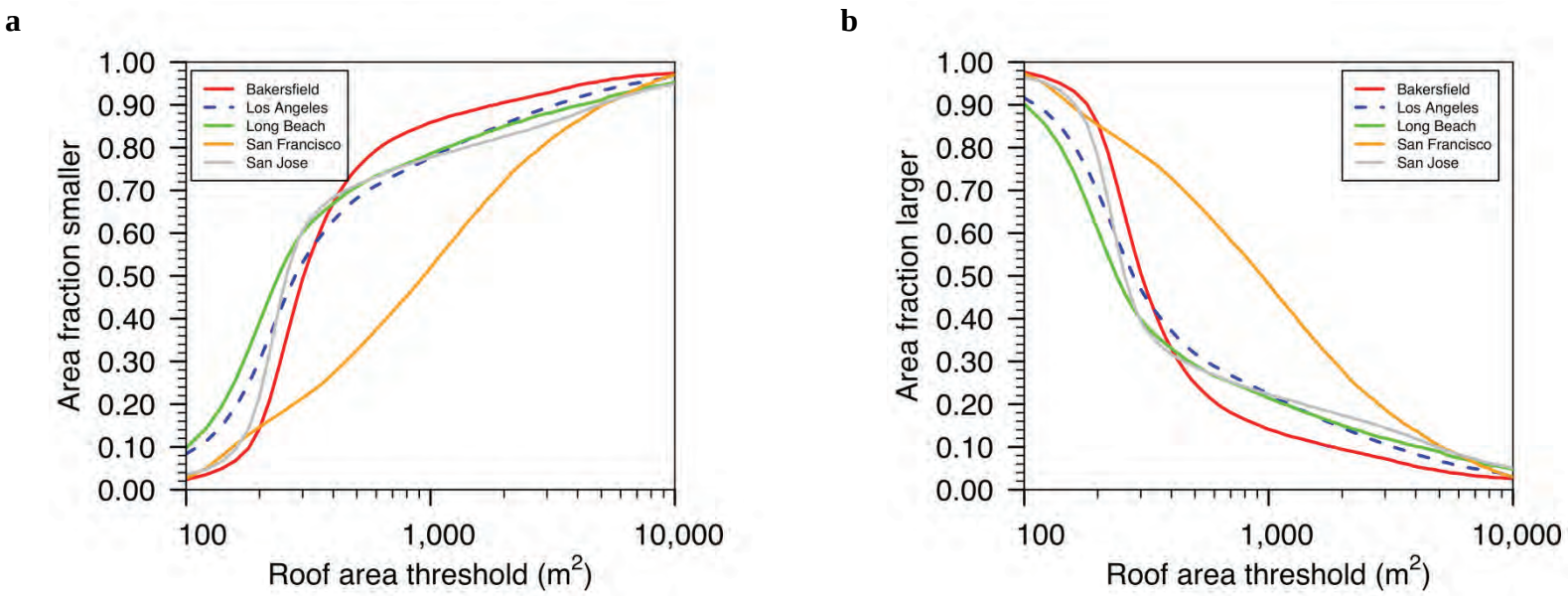

Figure 4-12. Fraction of urban roof area comprised of roofs that are (a) smaller and (b) larger than a range of roof area thresholds. Also shown are mean albedos for all roofs (c) smaller and (d) larger than the roof area thresholds. Mean albedos are weighted by roof area.

c

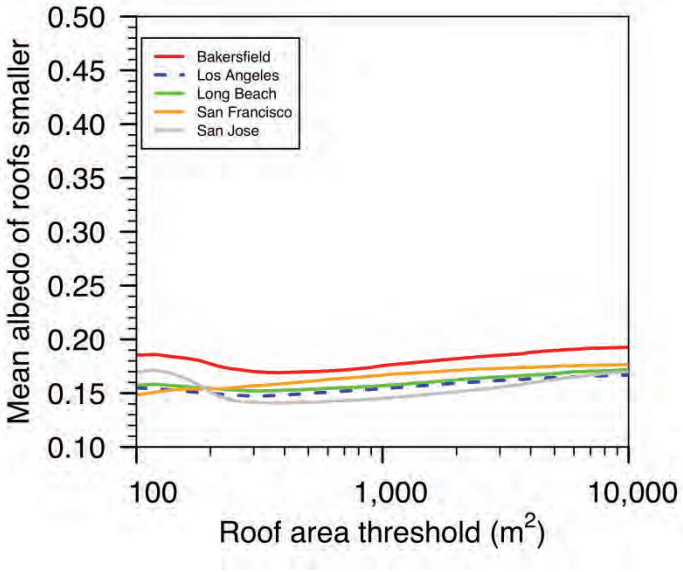

d

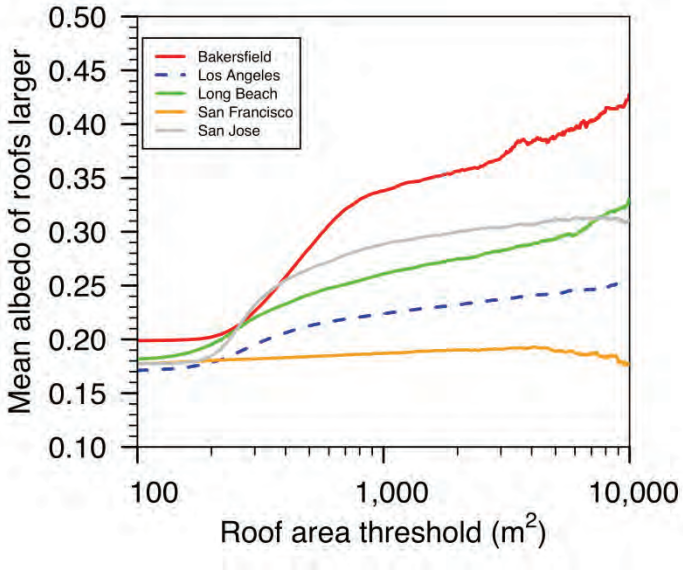

Figure 4-12 (continued)

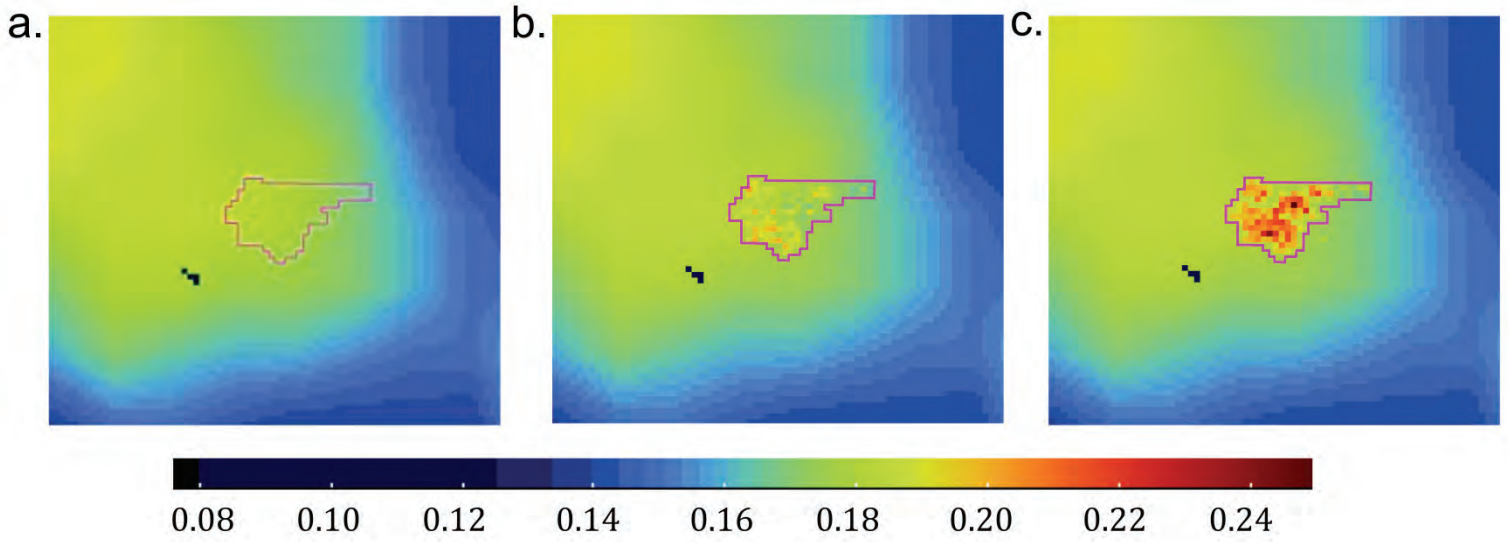

Figure 4-13. Surface albedos accounting for all land cover types used as an input to the meteorological model (WRF). Default albedos derived using only MODIS observations are in (a). Albedos used in the 'base_case' and 'cool_roof' scenarios are in (b) and (c). The magenta line shows Bakersfield city limits. Black cells southwest of Bakersfield indicate water.

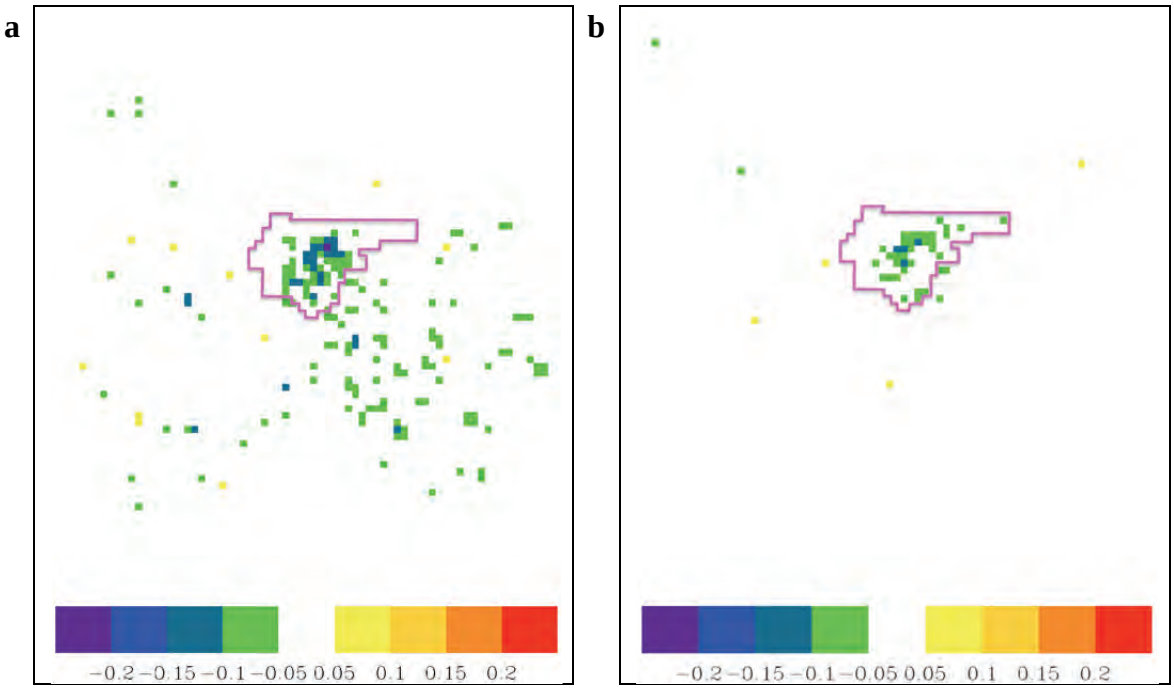

Figure 4-14. Mean change in summer (a) and winter (b) air temperature due to cool roofs, computed as ‘cool_roof’ minus ‘base_case’ scenarios. Temperatures are diagnosed as 2 meter air temperature at 15:00 LST. Only changes that are significant at the 95% confidence level are shown.

5. Summary and conclusions

In this report we have presented a method for deriving the mean albedo of individual roofs in California using aerial imagery. The imagery was acquired on an airplane at high spatial resolution (1 m) in four spectral bands (three in the visible and one in the near-IR) using a radiometrically calibrated sensor. Including the near-IR band is important for quantifying roof albedo since (1) some "cool roofs" have low reflectance in the visible but high reflectance in the near-IR, and (2) about 50% of the energy from the sun is in the near-IR part of the solar spectrum. We have developed methods for (a) identifying building outlines, (b) converting the four narrowband reflectances to solar reflectance (albedo) based on laboratory measurements of solar spectral reflectance for 190 roofing products, and (c) calibrating remotely sensed albedos by comparing to measured albedos of several roofs in each city.

We characterize the albedos of individual roofs for seven cities in California: Los Angeles, Long Beach, Bakersfield, San Francisco, San Jose, Sacramento, and San Diego (Table 4-1). In the first five cities we report roof albedos for every building within city boundaries, while for the latter two cities we describe on a statistically representative sample of buildings. Using Monte Carlo simulations we randomly sampled from the population of ~1.1 million roofs in Los Angeles to show that 1000 roofs was sufficient for characterizing the mean albedo of a city.

The mean roof albedo (weighted by roof area) for five of the seven cities was 0.17 ± 0.08 to 0.20 ± 0.11 (Los Angeles, Long Beach, San Francisco, San Jose, Bakersfield). The mean roof albedo was slightly higher in Sacramento (0.24 ± 0.11) and even greater in San Diego (0.29 ± 0.15) (Table 4-1).

California public policy that was implemented in 2005 (CEC 2005) requires that new or retrofitted low slope roofs on non-residential buildings should in many cases have high albedo. (See Appendix B for more details on cool roof policies in California.) Roof albedo results presented here were used to estimate the fraction of these roofs that had high albedo in 2009. Since identifying non-residential buildings with low slope roofs was beyond the scope of this study, buildings with footprint area > 5000 m^2 were used as a proxy. The fraction of this subset of buildings with roof albedo > 0.4 varied by city from 3 to 41%. Limitations of this calculation are in Section 4.3.2.

Buildings with small roofs, which are presumably mostly residential homes, represented a large fraction of total city roof area. For example, roofs with area < 400 m^2 made up about 60-70% of total roof area while roofs with area >1000 m^2 made up only about 15-25% in Los Angeles, Long Beach, San Jose, and Bakersfield. In these cities, roofs with area < 400 m^2 had low city-wide mean albedos ranging from 0.14 to 0.17. Thus, the majority of roof area was made up of small roofs with low albedo. This suggests that increasing the albedo of small (presumably residential) roofs could be an effective way of increasing urban albedo. We note that there exist "cool colored" roofs with relatively high albedo that are dark in the visible but have high reflectance in the near-IR part of the spectrum. This design allows the roof to maintain a dark appearance while increasing its

albedo. Cool colored roofing products exist with albedos of up to about 0.40. As a point of comparison, white roofs are available with albedos of about 0.90 (CRRC, 2013).

A regional climate model was used to simulate potential temperature changes attainable by converting the current stock of roofs in Bakersfield to cool roofs. Simulations indicated that average afternoon (15:00 LST) temperatures could be reduced by up to 0.2 °C during both the summer and winter. Statistically significant temperature changes were simulated downwind (southeast) of Bakersfield during summer. Cool roofs did not induce statistically significant changes in precipitation.

Temperature changes modeled in this investigation are smaller than changes predicted by past studies for other cities in California (e.g. Taha 2008b). These discrepancies in temperature change are due in part to differences in study design. First, assumed albedo increases in our investigation were from cool roofs only, while Taha also included contributions from cool walls and pavements. A second difference is that Taha reported temperature changes for a four-day high ozone episode, whereas temperature changes reported here are averaged over 10 model weeks per season (2 weeks per season × 5 years). By averaging over this longer time period we are representing climatic seasonal means instead of a particular meteorological regime. We also note that neither study considered the influence of increased urban vegetation on urban climate.

This project resulted in the creation of shapefiles containing outlines and mean roof albedos for every building in Los Angeles, Long Beach, San Francisco, San Jose, and Bakersfield. For Sacramento and San Diego, these shapefiles were created for a reduced but statistically representative sample of buildings (N~1000).

5.1. Future Research

We recommend a few follow up studies. First, the roof albedo databases described here can serve as inputs to climate models as described in Section 4.4 . While this section presented climate simulations for Bakersfield, future studies should use the roof albedos in this report to model the climate impacts of increasing roof albedos in other California cities.

Future work should use the approach described in this report to determine the albedos of pavement surfaces and urban vegetation at the scale of entire cities in California. These are important inputs to climate models and would also permit calculation of the possible albedo increases attainable from cool pavements and increased vegetation.

In addition, for Sacramento and San Diego we reported albedos of a small but statistically representative sample of roofs. When city-wide building outlines become available for these cities, we recommend applying the method presented in this report to all roofs. While analyzing all roofs should not appreciably change the mean roof albedos of each city, these data are inputs required by climate models.

Lastly, we recommend repeating the analysis presented here in future years to track increased adoption of high albedo roofs.

6. References

Akbari H, Rosenfeld A, Taha H (1990). Summer heat islands, urban trees, and white surfaces. In *Proceedings of the 1990 ASHRAE Winter Conference*. http://isswprod.lbl.gov/library/view-docs/public/output/LBL-28308.pdf.

Akbari H, Davis S, Dorsano S, Huang J (1992). Cooling Our Communities: A Guidebook on Tree Planting and Light-Colored Surfacing. A Report to the United States Environmental Protection Agency. Report number 22P.2001. http://escholarship.org/uc/item/98z8p10x.

Akbari H, Bretz S, Taha H, Kurn D, Hanford J (1997). Peak power and cooling energy savings of high-albedo roofs. *Energy and Buildings*, 25, 117–126.

Akbari H, Rose LS, Taha H (1999). Characterizing the Fabric of the Urban Environment: A Case Study of Sacramento, California. Lawrence Berkeley National Laboratory Report LBNL-44688, Berkeley, CA. doi:10.2172/764362.

Akbari H, Pomerantz M, Taha H (2001). Cool surfaces and shade trees to reduce energy use and improve air quality in urban areas. *Solar Energy*, 70, 295–310.

Akbari H, Rose LS (2001a). Characterizing the fabric of the urban environment: a case study of metropolitan Chicago, Illinois. Lawrence Berkeley National Laboratory Report LBNL-49275, Berkeley, CA. http://repositories.cdlib.org/lbnl/LBNL-49275.

Akbari H, Rose LS (2001b). Characterizing the fabric of the urban environment: a case study of Salt Lake City, Utah. Lawrence Berkeley National Laboratory Report LBNL-47851, Berkeley, CA. http://escholarship.org/uc/item/0wk718sm.

Akbari H, Rose LS, Taha H (2003). Analyzing the land cover of an urban environment using high-resolution orthophotos. *Landscape and Urban Planning*, 63, 1–14.

Akbari H (2003). Measured energy savings from the application of reflective roofs in two small non-residential buildings. *Energy*, 28, 953–967.

Akbari H, Levinson R, Rainer L (2005). Monitoring the energy-use effects of cool roofs on California commercial buildings. *Energy and Buildings*, 37, 1007–1016.

Akbari H, Rose LS (2008). Urban Surfaces and Heat Island Mitigation Potentials. *Journal of the Human-Environmental System*, 11, 85–101.

Akbari H, Menon S, Rosenfeld A (2009). Global cooling: increasing world-wide urban albedos to offset CO2. *Climatic Change*, 94, 275–86.

Akbari H, Matthews HD, Seto D (2012). The long-term effect of increasing the albedo of urban areas. *Environmental Research Letters*, 7, 1-10.

ASTM (2006) ASTM Standard E1918-06, Standard Test Method for Measuring the Solar Reflectance of Horizontal and Low-Sloped Surfaces in the Field, ASTM International, West Conshohocken, PA.

Ban-Weiss GA, Wray C, Delp W, Ly P, Akbari H, Levinson R (2013). Electricity production and cooling energy savings from installation of a building-integrated photovoltaic roof on an office building. Energy and Buildings, 56, 210-220.

Beisl U, Telaar J, Schönermark MV (2008). Atmospheric correction, reflectance calibration and BRDF correction for ADS40 image data. *The International Archives of the Photogrammetry, Remote Sensing and Spatial Information Sciences, Vol. XXXVII, Part B7,* http://isprsserv.ifp.uni-stuttgart.de/proceedings/XXXVII/congress/7_pdf/1_WG-VII-1/02.pdf .

Beisl U, Adiguezel M (2010). Validation of the reflectance calibration of the ADS40 airborne sensor using ground reflectance measurements. *ISPRS TC VII Symposium – 100 Years ISPRS, Vienna, Austria, July 5–7, 2010, IAPRS, Vol. XXXVIII, Part 7B,* http://www.isprs.org/proceedings/XXXVIII/part7/b/pdf/80_XXXVIII-part7B.pdf .

Campra P, Garcia M, Canton Y and Palacios-Orueta A (2008). Surface temperature cooling trends and negative radiative forcing due to land use change toward greenhouse farming in southeastern Spain. *Journal of Geophysical Research*, 113, D18109. doi:10.1029/2008JD009912.

CEC (2005). California Energy Commission Building Energy Efficiency Standards, For Residential and Nonresidential. Publication # CEC-400-2006-015 http://www.energy.ca.gov/2006publications/CEC-400-2006-015/CEC-400-2006-015.PDF.

CEC (2008). California Energy Commission Building Energy Efficiency Standards, For Residential and Nonresidential. Publication # CEC-400-2008-001-CMF. http://www.energy.ca.gov/2008publications/CEC-400-2008-001/CEC-400-2008-001-CMF.PDF

CEC (2013). California Energy Commission Building Energy Efficiency Standards, For Residential and Nonresidential. Publication # CEC-400-2012-004-CMF-REV2. http://www.energy.ca.gov/2012publications/CEC-400-2012-004/CEC-400-2012-004-CMF-REV2.PDF

City and County of San Francisco (2011). San Francisco Data. Building Footprints. Obtained in 2011 at https://data.sfgov.org/.

City of Bakersfield (2011). Geographic Information Services. Obtained in 2011 at http://www.bakersfieldcity.us/gis/downloads/.

City of San Jose (2011). GIS/Public Works. Building outlines for 2006. Obtained in 2011 by personal communication with Vicky Gallardo**,** Senior Geosystems Specialist.

CRRC (2013). Cool Roof Rating Council Rated Products Directory, http://coolroofs.org.

Downey M, Uebbing R, Gehrke S, Beisl U (2010). Radiometric processing of ADS imagery: using atmospheric and BRDF corrections in products. *ASPRS 2010 Annual Conference*, San Diego, CA. http://www.asprs.org/a/publications/proceedings/sandiego2010/sandiego10/Downey.pdf.

Georgescu M, Mahalov A, Moustaoui M (2012). Seasonal hydroclimatic impacts of Sun Corridor expansion. *Environmental Research Letters,* 7, 1-9.

Hyslop NP, White WH (2009). Estimating precision using duplicate measurements, *Journal of the Air and Waste Management Association,* 59, 1032-1039. doi:10.3155/1047-3289.59.9.1032

Jacobson MZ, Ten Hoeve JE (2012). Effects of urban surfaces and white roofs on global and regional climate. *Journal of Climate,* 25, 1028-1044.

Konopacki S, Akbari H (2001). Measured energy savings and demand reduction from a reflective roof membrane on a large retail store in Austin. Lawrence Berkeley National Laboratory Report LBNL-47149, Berkeley, CA. doi:10.2172/787107.

Liang S (2000). Narrowband to broadband conversions of land surface albedo I algorithms. *Remote Sensing of Environment*, 76, 213-238.

Liang S, Shuey CJ, Russ AL, Fang H, Chen M, Walthall CL, Daughtry CST, Hunt Jr. R (2002). Narrowband to broadband conversions of land surface albedo: II. Validation. *Remote Sensing of Environment,* 84, 25–41.

Leica (2013). Leica ADS80 Airborne Digital Sensor Digital Airborne Imaging Solution. http://www.leica-geosystems.com/downloads123/zz/airborne/ads80/brochures-datasheet/ADS80_datasheet_en.pdf.

Levinson R, Akbari H (2010). Potential benefits of cool roofs on commercial buildings: conserving energy, saving money, and reducing emission of greenhouse gases and air pollutants. *Energy Efficiency,* 3, 53–109.

Levinson R, Akbari H, Berdahl P (2010). Measuring solar reflectance—Part I: Defining a metric that accurately predicts solar heat gain. *Solar Energy*, 84, 1717–1744.

Levinson R, Berdahl P, Abkari H, Miller W, Joedicke I, Reilly J, Suzuki Y, Vondran M (2007). Methods of creating solar-reflective nonwhite surfaces and their application to residential roofing materials. *Solar Energy Materials & Solar Cells*, 91, 304-314.

Los Angeles Region Imagery Acquisition Consortium 3 (2011). LAR-IAC3, http://planning.lacounty.gov/LARIAC/lariac3Main.htm.

Lynn BH, Carlson TN**,** Rosenzweig C**,** Goldberg R**,** Druyan L**,** Cox J**,** Gaffin S**,** Parshall L**,** Civerolo K (2009). A modification to the NOAH LSM to simulate heat mitigation

strategies in the New York City metropolitan area. *Journal of Applied Meteorology and Climatology*, 48, 199–216.

Markelin L, Honkavaara E, Beisl U, Korpela I (2010). Validation of the radiometric processing chain of the LEICA ADS40 airborne photogrammetric sensor. *ISPRS TC VII Symposium – 100 Years ISPRS, Vienna, Austria, July 5–7, 2010, IAPRS, Vol. XXXVIII, Part 7A.* http://www.isprs.org/proceedings/XXXVIII/part7/a/pdf/145_XXXVIII-part7A.pdf.

Menon S, Akbari H, Mahanama S, Sednev I, Levinson R (2010). Radiative forcing and temperature response to changes in urban albedos and associated CO_2 offsets. *Environmental Research Letters*, 5, 1-11.

Millstein D, Menon S (2011). Regional climate consequences of large-scale cool roof and photovoltaic array deployment. *Environmental Research Letters*, 6, 1-9.

NAIP (2013). National Agriculture Imagery Program, United States Department of Agriculture's Farm Service Agency (FSA). http://www.fsa.usda.gov/FSA/apfoapp?area=home&subject=prog&topic=nai.

Oleson KW, Bonan GB, Feddema J (2010). Effects of white roofs on urban temperature in a global climate model. *Geophysical Research Letters*, 37. doi:10.1029/2009GL042194.

Parker DS, Barkaszi Jr. SF, Chandra S, Beal DJ (1995). Measured cooling energy savings from reflective roofing systems in Florida: field and laboratory research results. In *Proceedings of the Thermal Performance of the Exterior Envelopes of Buildings VI*, Clearwater, FL, December 4–8.

Parker DS, Sherwin JR, Sonne JK (1998). Measured performance of reflective roofing systems in a Florida commercial building. In *American Society of Heating, Refrigeration, and Air Conditioning Engineers*, Atlanta, Georgia, January, *ASHRAE Transactions*, 104, 1.

Pomerantz M and Akbari H (1998). Cooler paving materials for heat island mitigation. Proceedings of the 1998 ACEEE Summer Study on Energy Efficiency in Buildings, Volume 9. http://www.aceee.org/files/proceedings/1998/data/index.htm

Pomerantz M, Akbari H, Chen A, Taha H, Rosenfeld AH (1997). Paving materials for heat island mitigation. Lawrence Berkeley National Laboratory Report No. LBL-38074, Berkeley, CA. doi:10.2172/291033

Pomerantz M, Akbari H, Harvey JT (2000a). Cooler reflective pavements give benefits beyond energy savings: durability and illumination. Lawrence Berkeley National Laboratory Report No. LBNL-43443, Berkeley, CA. http://www.escholarship.org/uc/item/85f4j7pj

Pomerantz M, Pon B, Akbari H, Chang S-C (2000b). The effect of pavement temperatures on air temperatures in large cities. Lawrence Berkeley National Laboratory Report No. LBNL-43442, Berkeley, CA

Rose LS, Akbari H, Taha H (2003). Characterizing the fabric of the urban environment: a case study of greater Houston, Texas. Lawrence Berkeley National Laboratory Report LBNL-51448, Berkeley, CA, http://repositories.cdlib.org/lbnl/LBNL-51448.

Rosenfeld A, Akbari H, Bretz S, Fishman B, Kurn D, Sailor D, Taha H (1995). Mitigation of urban heat islands: materials, utility programs, updates. *Energy & Buildings*, 22, 255-265.

Schaaf CB, Gao F, Strahler AH, Lucht W, Li XW, Tsang T et al. (2002). First operational BRDF, albedo nadir reflectance products from MODIS. *Remote Sensing of Environment*, 83, 135-148.

Schaaf CB (2004). MODIS BRDF/Albedo Product (MOD43B) User's Guide, http://www-modis.bu.edu/brdf/userguide/albedo.html. See also http://modis-atmos.gsfc.nasa.gov/ALBEDO/.Slaton MR, Hunt Jr ER, Smith WK (2001). Estimating near-infrared leaf reflectance from leaf structural characteristics. *American Journal of Botany*, 88, 278-284.

Skamarock WC, Klemp JB, Dudhia J, Gill D, Barker D, Duda M, Huang XY, Wang W, Powers J (2008). A description of the advanced research WRF version 3 NCAR Technical Note NCAR/TN-475+STR, Boulder, CO. National Center for Atmospheric Research. http://www.mmm.ucar.edu/wrf/users/pub-doc.html

Sleiman M, Ban-Weiss GA, Gilbert H, Francois D, Berdahl P, Kirchstetter T, Destaillats H, Levinson R (2011). Soiling of building envelope surfaces and its effect on solar reflectance-part I: analysis of roofing product databases. *Solar Energy Materials and Solar Cells*, 95, 3385-3399.

Synnefa A, Dandou A**,** Santamouris M**,** Tombrou M, Soulakellis N (2008). On the use of cool materials as a heat island mitigation strategy. *Journal of Applied Meteorology and Climatology*, 47, 2846–56.

Taha H, Akbari H, Rosenfeld A, Huang J (1988). Residential cooling loads and the urban heat island–the effects of albedo. *Building and Environment*, 23, 271-283.

Taha H (2008a). Urban surface modification as a potential ozone air-quality improvement strategy in California: a mesoscale modelling study. *Boundary Layer Meteorology*, 127, 219–39.

Taha H (2008b). Meso-urban meteorological and photochemical modeling of heat island mitigation. *Atmospheric Environment*, 42, 8795–8809.

Taha H (2008c). Episodic performance and sensitivity of the urbanized MM5 (uMM5) to perturbations in surface properties in Houston Texas. *Boundary Layer Meteorology*, 127 193–218.

Zhou Y, Shepherd JM (2009). Atlanta's urban heat island under extreme heat conditions and potential mitigation strategies. *Natural Hazards*, 52, 639–668.

Appendix A. Estimating the potential for cool roofs to increase urban albedo

The results presented in Figure 4-12 can be used to estimate the roof albedo increase, ΔS, that could be attained in a city by converting all roofs of a particular size range to reflective roofs. That is,

$$\Delta S = F(S_{\text{cool}} - S_{\text{current}}) \qquad \text{(A-1)}$$

where F is the fraction of total roof area covered by roofs in a size range, S_{current} is the current albedo of roofs in that size range, and S_{cool} is the assumed cool roof albedo attainable in that size range. To compute the albedo change possible by converting all roofs below a given size threshold, values from Figure 4-12a,c should be used for S_{current} and F, respectively. Alternatively, the roof albedo change possible by converting all roofs above a given size threshold can be computed using values from Figure 4-12b,d. For example, consider converting all roofs > 5000 m^2 in Los Angeles to white roofs. Roofs of this size account for 7% of total roof area (Figure 4-12d) and have a mean albedo of 0.23 (Figure 4-12b). The maximum 'aged' albedo (assuming 3 years of outdoor exposure) of currently available white roofs is about 0.85 (CRRC 2013). Therefore, the estimated maximum city-wide roof albedo increase attainable by converting roofs > 5000 m^2 in Los Angeles is 0.07 × (0.85 - 0.23) = 0.04. It should be noted that while these estimates are useful for computing potential city-wide albedo increases from roofs of different sizes, they do not highlight the fact that energy use benefits from reflective roofs are highly dependent on other building characteristics.

Appendix B. Brief summary of cool roof requirements in California

California's Title-24 Building Energy Efficiency Standards (or 'Energy Code') includes mandatory requirements, which specify practices that must be followed, and prescriptive requirements, that regulate the performance of each building component. First, all buildings must comply with all mandatory requirements. For both the 2005 (CEC 2005) and 2008 (CEC 2008) Energy Code, the mandatory requirements for roofing products specify the certification and labeling requirements for cool roofing products. Second, buildings must demonstrate energy efficiency through either 'prescriptive compliance', in which each component of the building meets a specific energy efficiency requirement, or via 'performance compliance', in which the annual energy use of the building is shown not to exceed that of prescriptive-compliant building of the same size, type, and location. The prescriptive compliance approach in the Energy Code includes requirements for cool roofing products.

In the 2005 Energy Code, only nonresidential buildings that pursued the prescriptive approach would be required to use cool roofs. The 2008 Energy Code added a prescriptive requirement for cool roofs on low-rise residential buildings.

The following summarizes the requirements for the prescriptive approach in the 2008 Energy Code. Nonresidential buildings with *low-slope* roofs in climate zones 2 through 15 must use cool roofs with an aged solar reflectance of at least 0.55. *High-slope* roofs that are "low density" (less than 5 lb/ft^2) in climate zones 2-16 must use cool roofs with aged solar reflectance of at least 0.20. *High-slope* roofs that are "high density" (5 lb/ft^2 or greater) must have an aged solar reflectance of at least 0.15 for all climate zones.

For low-rise residential buildings with *high-slope* roofs, the minimum aged solar reflectance is 0.20 for low density roofs in climate zones 10 through 15, and 0.15 for high density roofs in all climate zones. Further, low-rise residential buildings with *low-slope* roofs in climate zones 13 and 15 must have a minimum aged solar reflectance of 0.55.

The 2013 Energy Code (CEC 2013) has increasingly stringent cool roof provisions, but this version was not in effect in 2009 when the imagery was acquired for the current study. Also note that the California Green Building Standards (CALGreen) and associated voluntary "reach" standards (a.k.a. "Tiers") have additional cool roof provisions. Cities and counties can (and do) adopt these provisions as mandatory at the local level.